PROPERTIES OF CESIUM IODIDE WITH INTRINSIC POINT DEFECTS : A DENSITY FUNCTIONAL THEORY STUDY

BY

PETER CHERUIYOT KIRUI

A THESIS SUBMITTED IN PARTIAL FULFILMENT OF THE REQUIREMENTS FOR THE DEGREE OF MASTER OF SCIENCE IN PHYSICS TO THE SCHOOL OF SCIENCE OF UNIVERSITY OF ELDORET, KENYA.

2016

DECLARATION

Declaration by the Candidate

This thesis is my original work and has not been presented for a degree in any other University. No part of this thesis may be reproduced without prior written permission of the author and/ or University of Eldoret.

Kirui, Peter Cheruiyot

Signature: ..... Date: .....

SC/PGP/008/11

Declaration by the Supervisors

This thesis has been submitted for examination with our approval as University Supervisors.

Signature: ..... Date: .....

Prof. George O. Amolo,

University of Eldoret, Eldoret, Kenya.

Signature: ..... Date: .....

Dr. Nicholas W. Makau,

University of Eldoret, Eldoret, Kenya.

DEDICATION

This work is dedicated to my prayerful, caring and loving wife Vivian, my charming children; Mercy, Emmaculate, Gideon and Mitchell. Dedication also goes to brothers, sisters and friends for the encouraging advice during this study.

ACKNOWLEDGEMENTS

First and foremost, I thank God for my blessed life full of perseverance and patience which made every morning challenges overcomed with ease making this study achievable with all odds and valleys. My spiritual fathers; Mr. David K. Sigei of Cheborgei deliverance church , Mr. Paul Yegon of Roret deliverance church for his electronic biblical text messages and deliverance church Kenya at large for their visionary sermons and verses which inspired me to complete this work. I would like to acknowledge my supervisors Prof. George Amolo and Dr. Nicholas W. Makau, members of computational science group of University of Eldoret both past and present, some of whom include Mike Atambo, Dennis Magero, Victor Mengwa, Winny Mulwa, Patrick Vaati and Tolbert Ngeywo for their effort and time that has made this study what it is. I acknowledge Dr. Phillip Nyawere for his productive and informative discussions which really enhanced the scope of this study.

I thank the University of Eldoret in collaboration with the ICTP for organising schools, workshops and conferences that were of great importance to this work. In particular, I express my deep gratitude to my supervisors; Prof. GO. Amolo and Dr. NW. Makau who made sure that I attended Khartoum workshop on advances in material science (Sudan). The workshop really motivated me in this study.

I also would like to acknowledge teaching fraternity especially the principals by then; Mr. Davies Keter and Mr. Alfred Chelule of Mombwo secondary school, Mr. Said Sigei of Kaminjeiwet secondary school and the current principal Mr. Samwel Koech of Kamanamsim secondary school for giving me ample time and other resources when finalizing this study and Teachers Service Commission at large for granting me a study leave and funding to undertake this research.

I would like to acknowledge the National Commission for Science, Technology and Innovation which has funded some of the computational resources placed at the disposal of the computational research group of University of Eldoret, of which I am a member.

I also would like to acknowledge the Centre for High Performance Computing (CHPC) - South Africa and the University of Eldoret - Kenya for availing their computational resources that were used in this work.

ABSTRACT

Cesium Iodide is one of the fastest scintillators with a very short decay time of *16ns*. This has made the material to attract a lot of attention in research and imaging industry especially regarding how to make it a better scintillator as well as a detector. In spite of its obvious uses, some of its properties are not well understood. In this study, the structural and electronic properties have been studied using DFT and GW methods. Calculations using *ab-initio* methods together with defect formation energies and migration energies have been done for both cationic and anionic defects. The calculated lattice parameter of 4.551 $\AA$ agree well with experimental value of 4.567 $\AA$ which is a deviation of only -0.35 %. A direct band gap through gamma high symmetry direction of pristine CsI was calculated as 3.71 eV which is an underestimation of $\approx 40\%$ of the experimental value of 6.2 eV. GW method resulted in an improvement of the band gap to a value of 5.5 eV which is 11.29% below the experimental value. The presence of lattice defects in CsI crystal led to a significant change in the bonding environment of the crystal. However, this led to a downward bending of the CB edge by 0.02 eV which is insignificant, resulting to an effective band gap of 3.69 eV. Defect formation energies were studied too. It was found out that the interstitial formation energies for cation and anion were 0.4325 eV and 0.30 eV, respectively. Vacancy formation energies were 0.25 eV and 0.16 eV for the cation and anion, respectively. While Frenkel defect energies were also determined at infinite distances as 0.21 eV and 0.16 eV for cation and anion, respectively. The migration paths for vacancies have also been studied. In particular, anion migration energy is easiest in the $V_I < 100 >$ at -1.5050 eV while in the other low index directions $V_I < 110 >$ and $V_I < 111 >$ were calculated as -1.5048 eV and -1.5049 eV, respectively. Cation migration energy was also easiest in the $V_I < 100 >$ at -1.5254 eV and in the other low index directions $V_I < 110 >$ and $V_I < 111 >$ were calculated as -1.5253 eV and -1.5252 eV, respectively.

Contents

LIST OF TABLES

LIST OF FIGURES

LIST OF SYMBOLS AND ABBREVIATIONS

The following are the symbols and acronyms used in this thesis.

a_0	Lattice parameter
$\AA$	Angstroms
AgI	Silver Iodide
amu	Atomic mass unit
B_0	Bulk modulus
$B_0^{'}$	Pressure derivative
BCC	Body-centered cubic
BGO	Bismuth germanate
BS	Band structure
BSE	Bethe salpeter equation
BZ	Brillouin-Zone
CaF_2	Calcium Fluoride
Ca	Calcium
CB	Conduction Band
Cs	Cesium
CsI	Cesium Iodide
DOS	Density of states
DFT	Density Functional Theory
E-V	Energy-volume
eV	Electron volt
Ge	Germanium
GGA	Generalized Gradient Approximation

HOMO	Highest Occupied Molecular Orbital
I^-	Stable Iodide ion
I^{-*}	Excited Iodide ion
ICTP	International centre of theoretical Physics
KI	Potassium Iodide
K-S	Kohn-Sham
LDA	Local Density Approximation
LUMO	Lowest Unoccupied Molecular Orbital
mm	Millimeters
N	Number of nuclei
NaI(Tl)	Thallium doped Sodium Iodide
NaI	Sodium Iodide
NaCl	Sodium Chloride
NEB	Nudged elastic band
PMT	Photo multiplier tube
PDOS	Projected density of states
Q.E	Quantum Espresso
RbI	Rubidium Iodide
RPA	Random phase Approximation
Ry	Rydberg constant
sec	Seconds
UV	Ultraviolet
VB	Valence band
W	Screened coulomb interaction operator
XRD	X-ray Diffraction
3D	Three-dimensional

CHAPTER ONE

INTRODUCTION

1.1 Background

Cesium Iodide (CsI) falls in the group of compounds referred to as alkali halide crystals. Generally, halides constitute a large family of crystals with good scintillating properties (Wei, *et.al.*, 2004). CsI crystallizes at room temperature into simple cubic structure. Below 420K, CsI crystallizes in a Zinc blende structure while it crystallizes in a wurzite structure at 420K. Above 420k, it crystallizes in a body-centered cubic structure (Bernard, 1947). Other compounds with the same structure are Aluminium cobalt, Mercury Zianide, Beryllium copper and Magnesium Chloride (Wheeler, 1923). Unlike CsI, KI crystallizes in sodium chloride structure while AgI crystallizes depending on its temperature.

CsI has a high γ -ray stopping power due to its relative atomic density and atomic number making it quite useful in gamma ray detectors. It is also resistant to thermal and mechanical shock (Ying, *et.al.*, 2009). The crystal can slightly absorb water vapour from the atmosphere and has a very short decay time (16ns), making it suitable for fast timing applications (Nagarkar, *et.al.*, 1998).

CsI is relatively soft, it does not cleave and can withstand rapid temperature changes.

Previous works on doped and undoped alkali halide crystals (Steven, 1998) have not considered extensively the effects of defects in crystals especially CsI. The clarification of these drawbacks to a great extent relies on carrying out systematic *ab-initio* calculations. In this study, a quantum mechanical approach on electronic structure i.e, (band structure and density of states), defect formation and migration energies are carried out with a view to addressing some of the key properties of CsI with different defects.

1.2 Scintillation

As radiation interacts with matter, it looses energy by ionizing or exciting matter. However, only a few materials have the right properties to allow the collection of the primary ionization from atomic radiation through electronic transition.

If the ionization is not preserved and collected, the electron or positive ion pairs are expected to recombine eventually. During this recombination, the energy used to separate the charges will be re-emitted to the surroundings as lattice vibrations and heat. Occasionally, a triplet electronic excited state is populated and the energy from such states is released as visible photons. This emission is known as atomic or molecular fluorescence. If this emission is caused by exciting radiation (visible light), it is called scintillation. The wavelengths of the fluorescent photons from the excited states are characteristic of the material and range from UV to red colour. These visible, secondary photons can be easily detected and amplified with photo multiplier tube. The details of the scintillation process depends very much on the molecular structure of the scintillator, which can easily be affected by the presence of defects.

A scintillation detector is a device that consists of a scintillator and a light detector usually a photo multiplier tube (PMT) (see figure 1.1).

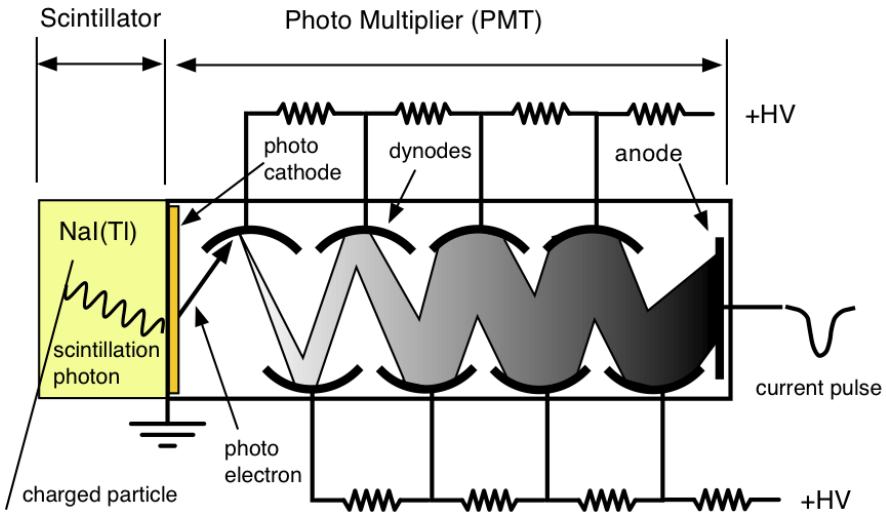

Figure 1.1: Scintillation process (Vladimir, 2007).

Scintillation detectors are used to detect nuclear radiations for instance in nuclear medicine and other applications. The role of a scintillator is to convert the energy that the ionizing radiation has lost into pulses of light. This relies to a great extend on the material's band structure.

1.3 Detectors

In a radiation detector, a fraction of the energy deposited by the primary radiation in the detector is converted to light, which in turn, is converted into an electrical signal. The process is divided into three processes as mentioned below

1. Scintillation process itself (energy to light).

2. Collection of light.

3. Multiplication of the electrons to make a macroscopic signal.

When an energetic electron passes through the crystal, it may raise valence electrons from the valence band to the conduction band. The vacancy in the valence band resulting from this ionization is called a ”hole”, in the valence band. The electron in the conduction band and the hole in the valence band can migrate independently through the crystal. These have the best light output and linearity. They typically consist of high Z components meaning they have a high density, therefore favoring detection of γ-rays.

1.4 Scintillator key parameters

Key parameters required in a scintillator are high density (resulting in high stopping power), good light yield and with quick decay time. They should be cost effective with high effective atomic number (Glenn, 2010) and transparent enough for emitted light to reach the detector.

1.5 Statement of the problem

There is much literature of both experimental and theoretical work of the fluorite structured alkali halides such as Sodium Iodide (NaI) and Rubidium Iodide (RbI). However, there is little information on both experimental and theoretical work of simple cubic structured halides such as CsI. Previous work has not done much to understand properties of CsI in the presence of point defects. There is therefore a need to perform studies to better understand the properties of CsI in the presence of defects.

1.6 Significance of the Study

CsI is one of the alkali halides with high density and high γ-ray stopping power making it quite useful in radiation detection, high energy physics, safety inspection and geological explorations and hence its study is essential. The material is relatively soft, it does not cleave and can withstand rapid temperature changes making it suitable for design of cell windows and as a radiation detector. This study investigated defect formation and migration energies of CsI so as to bring a clear understanding of the energy necessary for the formation of these defects and how they influence CsI as a detector material.

1.7 Objectives

The overall objective was the study of structural and electronic properties as well as formation energies in CsI upon the introduction of intrinsic point defects, with the following specific objectives:

1. To calculate the structural properties of CsI using density functional theory.
2. To calculate the band structure and density of states of pure and defective CsI.
3. To calculate the formation energies of intrinsic point defects in CsI.
4. To determine the migration path energies for cations and anions in CsI from *ab-initio* methods and to calculate the migration energies in low index migration paths.

CHAPTER TWO

LITERATURE REVIEW

2.1 Introduction

The study of CsI dates back to 1968 (Yositaka, 1968) when the material was found to posses superior scintillating properties as compared to other akali halides such as NaI. It was however the work of Ribeiro *et al* (Ribeiro, *et.al.*, 2006) regarding the bulk and surfaces properties of CsI in 2006, that has rekindled greater attention on alkali halides especially their scintillation properties. Ribeiro and co-workers showed from their theoretical calculations that the crystal lattice constant, a_0 of CsI was 4.635 Å, a value which was 1.49 % off the experimental value of 4.567 Å, while the bulk modulus was 12.21 GPa, only 2.14 % off the experimental value of 11.9 GPa. Their calculated band gap of 3.9 eV was 63 % lower than the experimental value of 6.2 eV.

Other researchers have studied CsI as a photocathode (Carlos & Carl, 2007) where they calculated a band gap of 3.56 eV for CsI as compared to the experimental value of 6.2 eV. Their value was even lower than that of Ribeiro *et al* mentioned earlier. Amolo, GO. *et.al.*, 2006 studied proton bombardment of CsI and reported that structural aspects influence the primary excitonic defect production mechanism and the resulting defects. The work employed high radiation flux γ -ray doses and showed the presence of I_3^- aggregates. These workers were able to investigate experimentally both optical and raman spectroscopy of defect growth and annealing studies of alkali halides for the first time.

Kun-Dar, Li.(2008) *et. al* worked on theoretical study of the defect formation (vacancies, interstitials and Frenkel pairs) energy, and vacancy migration energy in Calcium Fluoride (CaF_2) where they observed cation and anion vacancy formation energies of 13.75 eV and 8.34 eV, respectively. The study found out that for cation, the second nearest neighbour Frenkel defects were stable and the defect formation energy was estimated to be 9.3 eV, while the third nearest neighbour Frenkel defect for Anion were stable and the formation energy was only 2.49 eV. They concluded that migration energy of cation vacancy in the $< 110 >$ direction of 3.93 eV was lower than that of $< 100 >$ of 4.62

eV. This study found that migration energy of cation vacancy in the $< 110 >$ direction of -1.5253 eV which was also lower than of $< 100 >$ direction of -1.5254 eV. Both studies suggested that the $< 110 >$ direction was the most likely path for Cation vacancies to migrate.

Annika and Packham (2014) have studied various inorganic scintillators such as CsI in comparison to organic scintillators. In their work they were able to report that the intensity, I,

$$I = I_o exp(-\mu d); \tag{2.1}$$

of mono energetic beam of γ-rays is reduced after entering the scintillator thickness, d (Kurt, E., *et.al.*, 2007) where the total linear attenuation coefficient μ is the sum of all interaction cross sections associated with the three basic processes of interaction between high-energy photon and matter namely, photoelectric effect, Compton interaction and pair production. The total attenuation coefficient as a function of energy can be compared between inorganic and organic scintillator materials as shown in Figure 2.1 which indicates

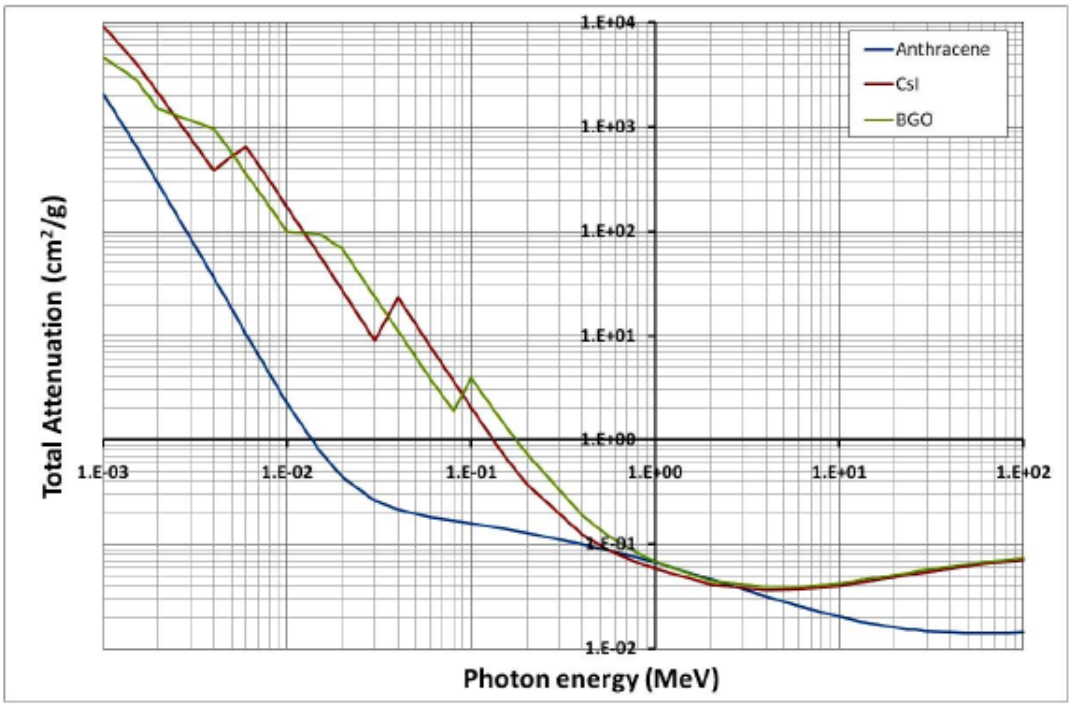

Figure 2.1: Total attenuation coefficients for three different scintillator materials(Hubbell & Seltzer, 2004).

quite clearly a high stopping power (greater attenuation length) for inorganic scintillator materials compared to organic ones. Scintillators such as CsI are insulators since they have a wide energy gap of 3.7 eV between the valence and conduction bands (Martin, 2005) as compared to the work of Ribeiro *et al* whose band gap was 3.9 eV who also used inorganic scintillator.

In this gap, Luminescence points/centers are found. The efficiency, η of inorganic scintillators can be approximated as,

$$\eta = \frac{E_s}{E_i}; \tag{2.2}$$

where E_s- Total energy of scintillation photons.

E_i- Energy deposited by the incident radiation.

The average amount of photons produced by every electron-hole pair depends on the transfer efficiency and light collection efficiency of the luminescence process in each scintillator. The energy efficiency η_{energy} is the combined efficiency of these two;

$$\eta_{energy} = \frac{\alpha}{\beta} \cdot \frac{h\nu_m}{E_g}; \tag{2.3}$$

where α -Average number of photons produced.

β- Numerical coefficient of the scintillator. For ionic crystals, β ranges between 1.5 and 2.0.

hν_m- Maximum energy of the emission spectrum and

E_g- Band gap width of the crystal.

2.2 Optical, structural and electrical properties of CsI

The crystal lattice of CsI (CsCl-type) takes a simple cubic structure when grown from the vapour phase on an appropriate single crystal substrate (Hirai, *et.al.*, 1998). CsI has a refractive index of 1.95 and photo-luminescence in the range of 310 nm to 420 nm with a light yield of 3.6 (Rihua, *et.al.*, 2007). As compared to other detectors, CsI has high quantum efficiency arising from a lower electron affinity and large electron escape length.

It has relatively high stability to ambient air and gas environments. The X-ray diffraction (XRD) patterns by sol-gel method shows an intense peak at 2 Θ of about 27.6^o which corresponds to the (110) preferred orientation of CsI and the evaporated film shows a (200) preferred crystallographic orientation. CsI films are opaque in the spectral range 190 to 225 nm, while in the spectral range 225 to 900 nm the films are transparent, with transmittance of over 80 % (Rihua, *et.al.*, 2007).

The atomic number of Cs is 55 and that of I is 53 which means Cs^+ has 54 electrons and I^- also has 54 electrons too. The ionic radius of Cesium is 1.81 $\AA$ while that of iodine is 2.06 $\AA$ (Itaru, *et.al.*, 2011). Thus, electronically the ions are identical and their scattering factors are similar. The diffraction pattern of CsI derives only from planes whose indice's sum is even (Jan, 2004), since the intensity of those planes whose indice's sum is odd is zero. Cesium Iodide is an insulator with high vapor pressure. When added to a mercury-free ultraviolet emitting metal halide lamp, there is reduction in temperature distribution inside the tube by restricting arc constriction due to ionization and dispersion effect. With respect to electric properties, potential gradient decreases as CsI is added and the amount of decrease in the potential gradient becomes larger as the amount of CsI is increased. This is due to the fact that CsI is an alkali halide crystal metal which is easy to ionize even on the arc wall, causing the arc to disperse (Bing, *et.al.*, 2009).

2.3 Point defects and defect migration

The conductivity of insulators is caused by the drift of ions. Although their drifts are smaller than in liquid phase, the ions are able to diffuse from site to site through the lattice. This drift is due to thermally created lattice defects (Arthur, 2002). The ionic conductivity, σ is given as;

$$\sigma_{ion} = N_{ion} e \varphi_{ion}, \tag{2.4}$$

where N_{ion} is the number of ions per unit volume that change their position , φ_{ion} is the mobility of these ions and e is the charge of the ion. N_{ion} depends on the vacancy concentration in the crystal (i.e., on the number of Schottky defects). The most common point defects are anion-Frenkel pairs i.e. anion vacancies and interstitial anions in the

cube-centre sites, with ionic transport occurring via the migration of the defects (Harry& Bishop, 2011). At temperatures just below melting point, T_m, the insulators exhibit a broad specific heat anomaly which passes through a maximum at a temperature, T_c. Ionic conductivity, σ, increases with temperature which in turn is increased by the presence of Schottky defects. For Schottky defects, vacancies allow other atoms to easily diffuse through them. Less energy is required to move the electrons and in the process, the vacancies migrate in the opposite direction.

This type of diffusion is an important property that helps in understanding whether it is possible that the defect can be incorporated during growth or processing. It also helps in the understanding of impurity diffusion, which is always mediated by native defects (Istratov & Weber, 2005). Defect formation energy, Δ E, is the energy required to create a defect and is related to the concentration of the defect, c, by the expression;

$$c = N_t exp(-\Delta E/K_B T), \tag{2.5}$$

where N_t is the total number of the sites in the lattice (per unit volume) in which the impurity can be incorporated, K_B is the Boltzman's constant and T is the temperature. In most ionic crystals, ΔE is much greater than K_BT even at the melting point, so that the defect concentration is always very small . This means that the number of vacancies increases with increase in temperature. Vacancies are normally created in pairs (e.g interstitial anion and anion vacancy) to allow the material to be neutral. Materials that contain a large number of defects, so that the ions can migrate easily (at high temperature T) also have a high ionic conductivity (Damian, *et.al.*, 2001).

CHAPTER THREE

THEORY

3.1 Defects in Materials

A structural defect is any fault in the long- or short-range order of a material. This applies to crystalline and non-crystalline solids having three-dimensional (3D) periodic structure (Catlow & Mackrodt, 1982). Defects are classified as either point or extended defects. Point defects includes imperfections which are localized over a few atomic sites, and they can be grouped as intrinsic and extrinsic point defects. Intrinsic point defects include vacancies (missing lattice atoms), interstitials (atoms occupying non-lattice sites). Various defects occur in crystalline solids, and include; point defects, line defects and bulk defects (see Figure 3.1).

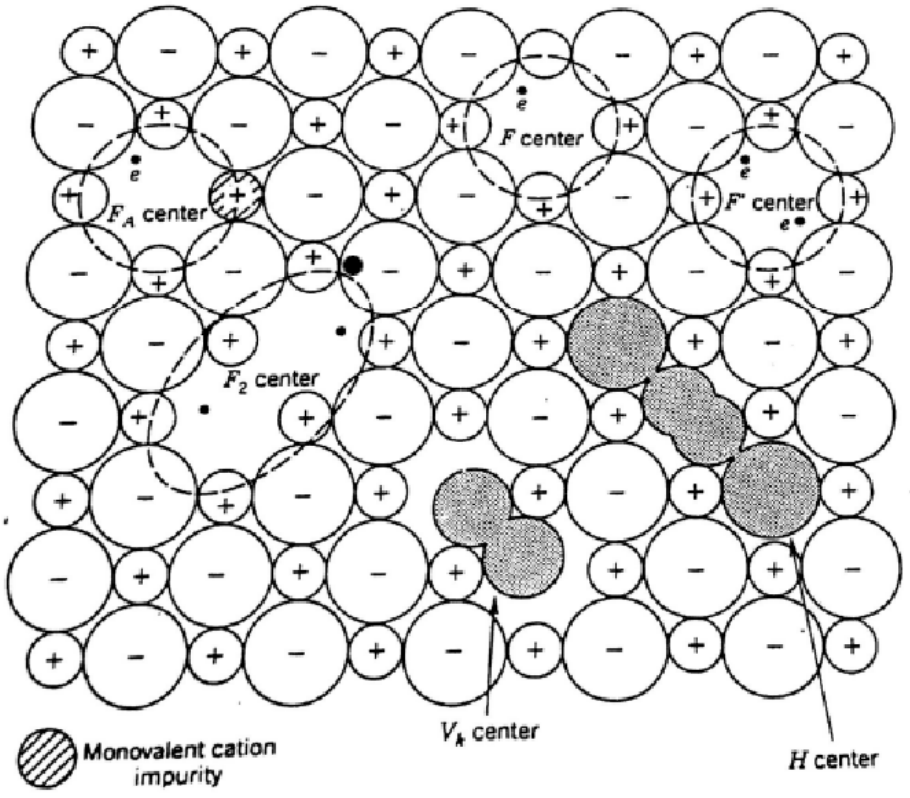

Figure 3.1: Common defects in alkali halides (William & Stoneham, 2004).

Extrinsic point defects arise from the presence of foreign atoms (William & Rethwisch, 2007).

Extended defects on the other hand influence large volumes of the material. For example a dislocation line may run throughout a crystal at the boundary of an arrangement in the lattice planes. Surfaces are examples of extended defects. During crystal growth, vacant lattice sites develop in all crystals. Such vacancies are stable at room temperature and may be mobile at slightly higher temperature. Once a vacant lattice site is developed, the immediate neighborhood of a vacancy will relax, perturbing several lattice sites (Shiyou, *et.al.*, 2010). If the vacancy is produced by displacing a lattice atom, then the released atom can either be trapped within the lattice (Frenkel defect) or moved out to the surface to form new crystal layers (Schottky defects) (Butman, *et.al.*, 2000). For the Frenkel defect, the displaced atom is retained in the interior of the crystal at an interstitial site.

3.1.1 Defect Migration

An activation energy E_m has to be supplied to an atom so that it could break inter-atomic bonds and to move into a new position (see Figure 3.2).

Considering the simple case of an atom moving into a vacancy and using the potential energy model proposed by Lidiard (Lidiard & McKee, 1980) i.e the potential energy is a function of displacement in the direction of the vacancy, the Hamiltonian for the atom may be expressed as,

$$H(x,p_x) = \frac{P_x^2}{2m} + V(x). \tag{3.1}$$

If the displacement x and momentum p_x are required for an atom to reach the saddle point for migration, then the probability of crossing the barrier is

$$P = \frac{\exp(-H(x,p_x)/kT)dxdp_x}{\int_{-\infty}^{\infty}\int_{-\infty}^{\infty}\exp(-H(x,p_x)/kT)dxdp_x}. \tag{3.2}$$

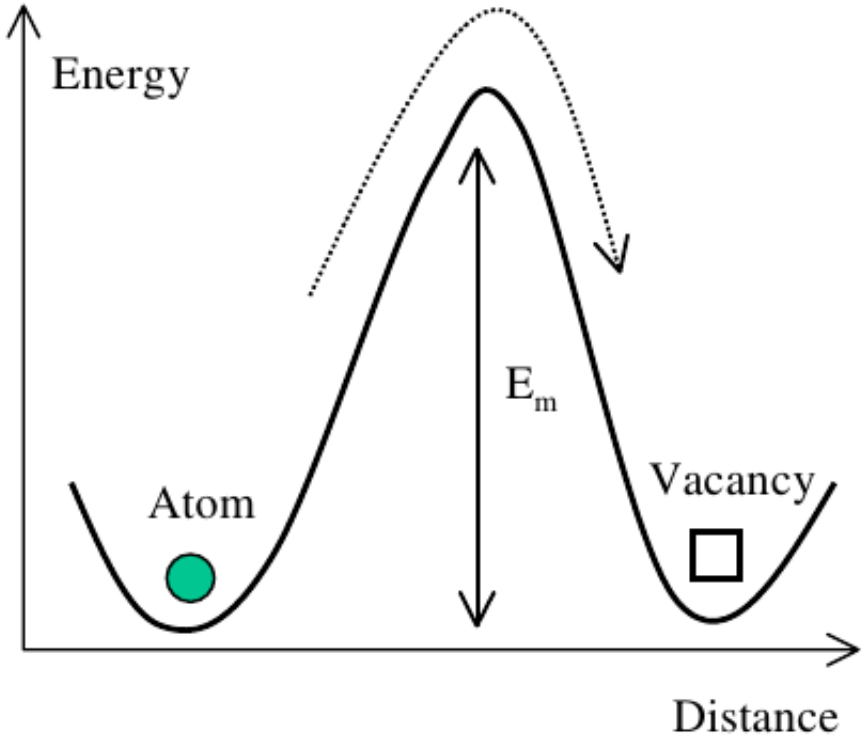

Figure 3.2: Schematic representation of diffusion of an atom from its original position into a vacant lattice site (Zhibin, *et.al*., 2008.)

(Kimerling, 1978). The fraction of atoms crossing the barrier in time dt is

$$vdt = dt\frac{\int_0^\infty \exp(-H(x,p_x)/kT)v_x dp_x}{\int_{-\infty}^{\infty}\int_{-\infty}^{\infty}\exp(-H(x,p_x)kT)dxdp_x}, \tag{3.3}$$

where $dx = v_x dt$ and v_x is the velocity of an atom at saddle point in the x direction of the vacancy. Equation 3.3 can further be expressed as,

$$\begin{aligned} vdt &= \frac{\frac{dt}{m}(mkT)\exp(-V(x)/kT)}{\int_{-\infty}^{\infty}\exp(-V(x)/kT)dx\int_{-\infty}^{\infty}\exp(-p_x/2mkT)dp_x} \\ &= \frac{dt\left[\frac{kT}{2\pi m}\right]^{\frac{1}{2}}\exp(-V(x)/kT)}{\int_{-\infty}^{\infty}\exp(-V(x)/kT)}. \end{aligned} \tag{3.4}$$

If the harmonic approximation potential is $V(x) = V(A) + kx^2/2$ then the fraction of atoms ϑ becomes,

$$\vartheta = \left[\frac{kT}{2\pi m}\right]^{\frac{1}{2}}\frac{\exp[-V(A)-V(x)/kT]}{(2\pi kT/k)^{\frac{1}{2}}}, \tag{3.5}$$

where A is the equilibrium position of the atom. Thus,

$$V(A) - V(x) = E_m, \tag{3.6}$$

where E_m = energy barrier for migration. Thus, the jump frequency ν associated with the vibration of the defect towards the saddle point at temperature T, is,

$$\nu = \frac{1}{2\pi}\left(\frac{k}{m}\right)^{\frac{1}{2}} \exp(-E_m/kT) \tag{3.7}$$

$$= \nu_0 \exp(-E_m/kT), \tag{3.8}$$

and to the best approximation its value is given by $\nu = kT/\hbar$ (Lindsey & Wales, 1999). Vineyard (Caglar, *et.al.*, 2009) while working independently of Damask and Dienes (Johnson, *et.al.*, 1964) have discussed the extension of the single defect model to include the interaction of the defect surrounding atoms and to allow for the return jump of the defect. This involves the construction of a configuration space in the region of the migrating atom (blue to red) and its potential trap (see figure 3.3).

Flux, J_1, from position (1) to (2) is written as,

$$J_1 = \frac{1}{2} n_1 \nu \tag{3.9}$$

where n_1 is the number of atoms at position 1,
ν is the jump frequency i.e number of atoms jumping per second. similarly,

$$J_2 = \frac{1}{2} n_2 \nu \tag{3.10}$$

where n_2 is the number of atoms at position 2,
ν is the jump frequency in s^{-1}. Accordingly the jump frequency can be expressed in the form of the ratio of two partition functions as

$$\nu = \left[\frac{kT}{2\pi}\right]^{\frac{1}{2}} \frac{\int_S \exp(-\phi/kT)dS}{\int_V \exp(-\phi/kT)dV}, \tag{3.11}$$

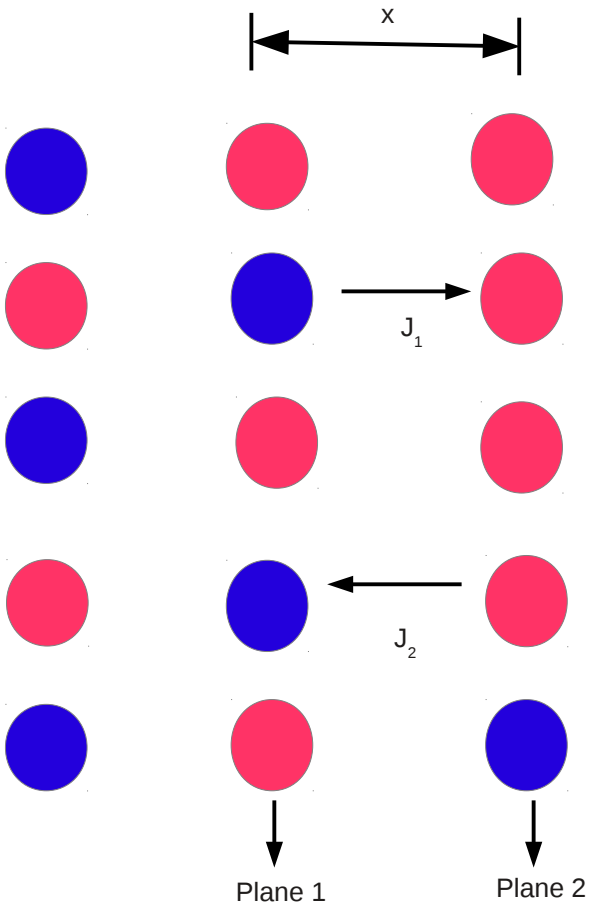

Figure 3.3: Schematic of the planes of atoms with arrows showing the cross-movement of the species (Paul, *et.al*., 2013).

where the integration in the numerator is over the hyper surface containing the saddle point and the integration in the denominator is over the configuration space on the defect side of the hyper surface. ϕ is the potential energy of the entire crystal. If equation (3.11) is expanded in a Taylor series about the defect(D) and also about the saddle point (P) the jump frequency becomes

$$\nu = \left[\frac{\prod_{j=1}^{N} \nu_j}{\prod_{j=1}^{N-1} \nu'_j}\right] \exp(-[\phi(P) - \phi(D)]/kT). \tag{3.12}$$

Hence the effective frequency ν_o is given by

$$\nu_0 = \left[\frac{\prod_{j=1}^{N} \nu_j}{\prod_{j=1}^{N-1} \nu_j{}'} \right] \tag{3.13}$$

and is the ratio of the product of N normal frequencies of the entire system at the starting point of the migration to the $N-1$ normal frequencies of the system in the saddle point configuration (Graeme, *et.al.*, 2002).

3.2 Many-body Approximations

3.2.1 Born-Oppenhelmer (B-O) Approximation

The Born-Oppenheimer approximation lightens the calculation of the energy and the wave function of moderate size physical systems by making use of the significant mass differences between the nuclei and the electrons. Considering the example of a methane molecule (Cawkwell & Niklasson, 2012) the mass of the nucleus is 2,800 times that of all the electrons surrounding it. It is therefore possible to decouple the motion of relatively slow moving nuclei and that of the fast moving electrons. In other words, the wave function of the system can be divided into electronic and nuclear components, i.e,

$$\psi(r,R) = \psi_{electronic}(r,R)\psi_{nuclear}(R). \tag{3.14}$$

In the first step of the Born-Oppenheimer Approximation (Simone, *et.al*., 2007) the nuclei are assumed to have fixed positions, and the electronic Schrodinger equation, which depends only on the electronic coordinates, is solved. For instance, the electronic wave function of the methane molecule depends on 30 electronic coordinates. It is assumed that for fixed nuclear positions, the electrons are in their ground state. Consequently, the calculated electronic energies are functions of nuclear positions. In the second step of the Born-Oppenheimer approximation, these electronic functions serve to calculate a potential for the nuclear component of the Schrödinger equation (Mauricio, *et.al*., 2003). In the case of the methane example, one needs to deal with only 15 variables. In general, the nuclei are considered to move on the potential energy surface of the electronic ground state, and the electrons follow the nuclear motion adiabatically.

3.2.2 Hatree Approximation

Here, the wave function is a product *ansatz* of the form :

$$\Psi(\vec{r_1},\vec{r_2},\ldots,\vec{r_N}) = \psi_1(\vec{r_1})\psi_2(\vec{r_2})\ldots\psi_N(\vec{r_N}), \tag{3.15}$$

whereby this is known as the independent-particle or Hartree approximation (John & Zunger, 1981). The wave function of the system is made up of a product of orthonormal molecular orbitals. In this case, the electrons only interact with a mean field created by all the other electrons, and they do not interact with other electrons directly. This approximation is computationally feasible, at least using self-consistent numerical methods. However, it is a crude approximation that fails to satisfy the Pauli exclusion principle for the many body wave function. Since the Pauli exclusion principle requires the wave function to be anti symmetric with respect to interchange of any two electron coordinates. This condition can not be satisfied by a non-trivial wave-function of the form given by equation 3.15.

3.2.3 Hatree-Fock Approximation

The Hartree-Fock approximation was an improvement on Hartree approximation that failed to represent the way in which particular (as opposed to the average) configuration of the $(N-1)$ electrons affects an electron under consideration. The Hartree-Fock approximation is viewed as the basis or foundation for more accurate approximations involving correlation between electrons (Janghwan, *et.al.*, 2009). Within the Hartree-Fock approximation, the many body wave function of the system can be treated as a single Slater determinant of independent electrons which satisfies the anti symmetry rule (Alexander, 2014). Hartree-Fock theory provides an exact treatment of the exchange and correlation, which are useful for calculations involving molecules and larger N-body systems (Yeong, 2014). Modification of the Hartree equation gives a Schrodinger-like equation with an effective Hamiltonian operator H^{i}_{eff} that depends on the state as,

$$H^{i}_{eff}\Psi(r) = \left(-\frac{\hbar^2}{2m_e}\nabla^2 + V^{i,\sigma}_{eff}(r)\right)\Psi^{\sigma}_{i}(r) = E^{\sigma}_{i}\Psi^{\sigma}_{i}(r). \tag{3.16}$$

The effective potential $V^{i,\sigma}_{eff}(r)$ that acts on each electron of spin σ at point r is expressed as in (Young-Choon, *et.al.*, 2012) that,

$$V^{i,\sigma}_{eff}(r) = V_{ext}(r) + V_{Hartree}(r) + V^{i,\sigma}_{x}(r), \tag{3.17}$$

where V_{ext} is the external potential, $V_{Hartree}$ is the Hartree potential and $V_x^{i,\sigma}$ is exchange potential. The exchange term operator $\mathrm{V}_x^{i,\sigma}$ is given by a sum over orbitals of the same spin as σ

$$V_x^{i,\sigma}(r) = -\sum_j \int dr' \Psi_j^{\sigma\star}(r') \Psi_i^{\sigma}(r') \frac{1}{|\mathbf{r}-\mathbf{r}'|} \frac{\Psi_j^{\sigma}(r)}{\Psi_i^{\sigma}(r)}. \tag{3.18}$$

The sum $\sum_i \Psi_j^{\sigma *}(r)\Psi_i^{\sigma}(r)$ is the Coulomb potential due to the exchange density for each state i, σ (Jan, 2001).

3.3 Density Functional Theory (DFT)

3.3.1 Introduction

Density Functional Theory (DFT) is an approach for investigating the electronic structure of atoms or molecules in solid state Physics and Chemistry. In its initial formalism, DFT is capable of covering the prediction of properties at ground state of any system of electrons, i.e at zero temperature and at zero pressure. It has relativistic extensions and in fact extensions to EM fields have already been achieved through DFT as well as to excited states through the so-called time dependent density functional theory (TDFT) (Yoshihiro, *et.al.*, 2004) . Several approximations are usually made in order to enable the computations to be accessible to current computers since more precision comes with more computational time. DFT is preferred in the study of solid state systems over other theoretical approaches (Eberhard & Dreizler, 2013), since it uses electronic density, n $(\vec{r})$ of the system which is much simpler to work with, as opposed to the 4N-dimensional wave functions. It is also preferred because it can be used in the study of both periodic and non-periodic systems.

3.3.2 Kohn-Sham(K-S) Equations

Kohn and Sham (K-S) (George, *et.al.*, 2013) derived a coupled set of differential equations enabling the ground-state density $n_0(\mathbf{r})$ to be found. K-S separated the ground-state

kinetic energy functional of a system of non-interacting electrons, $E[n(r)]$ into ,

$$E[n(r)] = T_0[n(r)] + E_H[n(r)] + E_{xc}[n(r)] + \int V_{ext}(r)n(r)d^3r, \tag{3.19}$$

where $T_0[n(r)]$, $E_H[n(r)]$ and $E_{xc}[n(r)]$ define the kinetic energy, Hartree energy as a consequence of electron-electron repulsion, and exchange and correlation energies, respectively. The functional E becomes

$$E\left[n(\mathbf{r})\right] = T_s\left[n(\mathbf{r})\right] + \frac{1}{2}\int\int \frac{n(\mathbf{r})n(\mathbf{r}')}{|\mathbf{r}-\mathbf{r}'|}d\mathbf{r}d\mathbf{r}' + E_{XC}n(\mathbf{r}) + \int n(\mathbf{r})V_{ext}(\mathbf{r})d\mathbf{r}, \tag{3.20}$$

where $T_s\left[n(\mathbf{r})\right]$ is the kinetic energy of a non-interacting electron gas with density $n(\mathbf{r})$, i.e.,

$$T_s\left[n(\mathbf{r})\right] = -\frac{1}{2}\sum_{i=j}^{N}\int \Psi_i^*(\mathbf{r}) \bigtriangledown^2 \Psi_i(\mathbf{r})d\mathbf{r} \tag{3.21}$$

$E_{XC}n(\mathbf{r})$ in equation (3.20) also defines the exchange-correlation energy functional. Introducing a normalization constraint on the electron density, $\int n(\mathbf{r})d\mathbf{r} = N$ gives

$$\begin{aligned} \frac{\delta}{\delta n(\mathbf{r})}\left[E\left[n(\mathbf{r})\right] - \mu\int n(\mathbf{r})\mathbf{dr}\right] &= 0 \\ \Rightarrow \frac{\delta E\left[n(\mathbf{r})\right]}{\delta n(\mathbf{r})} &= \mu. \end{aligned} \tag{3.22}$$

(John, *et.al.*, 1996) Equation (3.22) may now be rewritten in terms of an effective potential, $V_{eff}(\mathbf{r})$, as,

$$\frac{\delta T_s\left[n(\mathbf{r})\right]}{\delta n(\mathbf{r})} + V_{eff}(\mathbf{r}) = \mu, \tag{3.23}$$

where

$$V_{eff}(r) = e^2\int \frac{n(r)}{\left|r-r'\right|}d^3r + \frac{\delta E_{ex}[n]}{\delta n(r)} + V_{ext}(r). \tag{3.24}$$

More importantly, non-interacting electrons moving in an external potential $V_{eff}(\mathbf{r})$ would result in the same relation as (3.23) (Yoshihiro, *et.al.*, 2004). To obtain the ground state energy, E_0, and the ground state charge density, n_0, the one electron Schrodinger equation

$$\left(\frac{1}{2}\bigtriangledown_i^2 + V_{eff}(\mathbf{r}) - \varepsilon_i\right)\psi_i(\mathbf{r}) = \mathbf{0} \tag{3.25}$$

can be solved self-consistently with

$$n(\mathbf{r}) = \sum_{i=j}^{N} |\psi_i(\mathbf{r})|^2, \tag{3.26}$$

A self-consistent solution is required due to the dependence of $V_{eff}(\mathbf{r})$ on $n(\mathbf{r})$. Equations 3.17 through 3.24 provide a theoretically exact method for finding the ground state energy of an interacting system, provided the form of E_{XC} is known. Unfortunately, the form of E_{XC} is in general unknown and its exact value has been calculated for only a few very simple systems. In electronic structure calculations E_{XC} is usually approximated within the local density approximation (LDA) or generalized-gradient approximation (GGA) (Jianmin, *et.al.*, 2003).

3.3.3 Local Density Approximation (LDA)

Within the framework of the local density approximation (LDA) (Taedaehyeong, *et.al.*, 2014), the value of $E_{XC}[n(r)]$ is approximated by the exchange-correlation energy of an electron in a homogeneous electron gas of density n(r), so that,

$$E_{XC}^{LDA}[n(r)] = \int E_{XC}[n(r)]n(r)dr. \tag{3.27}$$

The LDA functional reproduces the ground state properties of many systems rather accurately. For example, (Korir, *et al*, 2011) showed in his work that the bulk properties of group 4d transition metals were well described by LDA, as opposed to other approaches. However, there are situations whereby LDA fails due to the manner in which it treats the charge density. For example, LDA predicts the wrong magnetic structure of iron. LDA has been superseded by Local Spin Density Approximation (LSDA), that expresses the density separately for electrons with spin up and those with spin down (Walter, 1999).

$$E_x^{LSDA}(n(\vec{r})) = \quad -\varepsilon_x \int \left(n_\uparrow^{4/3}(\vec{r}) + n_\downarrow^{4/3}(\vec{r}) \right) dr, \tag{3.28}$$

$$where: \varepsilon_x = 2^{1/3} C_x, \tag{3.29}$$

$$C_x = \tfrac{3}{4} \left(\tfrac{3}{\pi} \right)^{1/3}. \tag{3.30}$$

ε_x is the exchange-correlation coefficient and C_x is the density parameter in the system. In most cases, LSDA is implied whenever modern calculations refer to LDA. LDA predicts inaccurately the band gap of semiconductor materials (Yang, *et.al.*, 2007), and hence new methods are required for such cases like the generalized gradient approximation.

3.3.4 Generalized Gradient Approximation (GGA)

The Local Spin Density Approximation method is improved upon by considering the non-uniform electron gas (Stig & March, 2013). This approach includes information about the density of electrons, as well as the local gradient of this density. There are numerous ways to include the gradient of the density, and this has led to a number of different functionals, of which the most common are the Perdew-Wang (PW91) and Perdew-Burke-Ernzerhof (PBE) functionals (Scott, *et.al.*, 2013). Generally, all GGA methods depend only on the density and its derivative, and in addition the Fermi and Coulomb holes are required to integrate to -1 and 0 (Hagen, *et.al.*, 2006) respectively. For the PBE functional, the exchange factor is written as an enhancement factor multiplied onto the LSDA functional i.e,

$$\varepsilon_x^{PBE} = \varepsilon_x^{LDA} F(x), \tag{3.31}$$

$$F(x) = 1 + a - \tfrac{a}{1+bx^2}, \tag{3.32}$$

$$\text{where: } x = \tfrac{\nabla n(\vec{r})}{n(\vec{r})^{4/3}}. \tag{3.33}$$

The correlation part is written as an enhancement factor added to the LSDA functional (Ping, *et.al.*, 2012).

$$\varepsilon_c^{PBE} = \varepsilon_c^{LDA} + cf_3^3 ln\left[1 + dt^2\left(\frac{1+At^2}{1+At^2+A^2t^4}\right)\right], \tag{3.34}$$

$$where: A = d\left[exp\left(-\frac{\varepsilon_c^{LDA}}{cf_3^3}\right) - 1\right]^{-1}, \tag{3.35}$$

$$f_3(\zeta) = \frac{1}{2}\left[(1+\zeta)^{2/3} + (1-\zeta)^{2/3}\right], \tag{3.36}$$

$$t = \left[2(3\pi^3)^{1/3} f_3\right]^{-1} x. \tag{3.37}$$

The PBE functional has been slightly modified to improve performance for periodic systems, using Revised PBE , but at the cost of violating the exchange hole condition, whereby the exchange hole does not sum up to -1 as required.

3.3.5 Time Dependent Density Functional Theory (TDDFT)

Time dependent density functional theory (TDDFT) describes the excited state properties of a system by employing adiabatic approximation together with PBE functionals used for the ground state of the system (Mary, *et.al.*, 2009). It is based on the fact that the ground-state density of an electronic system uniquely determines external potential that the particles move in, which is associated with a specific Hamiltonian operator. This specific Hamiltonian operator fully describes the ground state as well as the excited states (Andres & Eva, 2006).

3.3.6 Bloch functions and plane wave basis

Bloch theorem states that the wave function of an electron within a perfectly periodic potential can be written as,

$$\psi_{nk}(r) = \mu_{nk} e^{ik.r,} \tag{3.38}$$

(David, *et.al.*, 2004) where k is the wave vector analogous to that of the wave vector in the theory of free electrons, r is a position vector, and $\mu_{nk}(r)$ is a periodic function that satisfies the boundary condition, $\mu_{nk}(r) = \mu_{nk}(r+R)$. The corresponding energy eigenvalue is,

$$\varepsilon_n(k) = \varepsilon_n(k+K), \tag{3.39}$$

where K is a reciprocal lattice vector. $\varepsilon_n(k)$ is a continuous function, and since the energies associated with the index, n, vary with wave vector, k, this is known as an energy band. All distinct values of $\varepsilon_n(k)$ are represented by k values within the first Brillouin Zone of the reciprocal lattice (Prasad & Bansil, 1980). The number of plane-waves used in a calculation is determined by:

$$\frac{\sqrt{E_{cutoff}2m_e}}{\hbar}, \tag{3.40}$$

where E_{cutoff} is the kinetic energy cut off. It is the only parameter that controls the accuracy of the plane wave basis set. Plane wave basis set are normally expressed as,

$$\psi(r) = \sum_j C_j \phi_j(r) \tag{3.41}$$

where ψ is a wave function and ϕ_j is a basis function (Mueni, 2014). They are mathematically simple, covering all the space equally without being biased to any particular region, and span the Hilbert space completely (Kosloff & Tal-Ezer, 1986). In this sense, they are superior to local basis sets, especially when the initial form of the wave functions is unknown.

3.4 G W Approximation

Defects are generally charged species in ionic and semi-ionic crystals, which owing to the long range of the Coulomb forces leads to a long-range relaxation field. Figure 3.4 shows a two-region method which can handle lattice relaxation around defects effectively (Kurt, 1953). It consists of a lattice surrounding the defect into an inner region (I) which is treated atomistically and in which the coordinates of all ions are adjusted until they are at ”zero force”, i.e. there are no net forces acting upon them. The method is essential for the region surrounding the defect where the defect forces are strong. The polarization P (r) at a point **(r)** with respect to the defect of charge q is given as,

$$P(r) = \frac{q\mathbf{r}}{r^3}(1 - \varepsilon^{-1}) \tag{3.42}$$

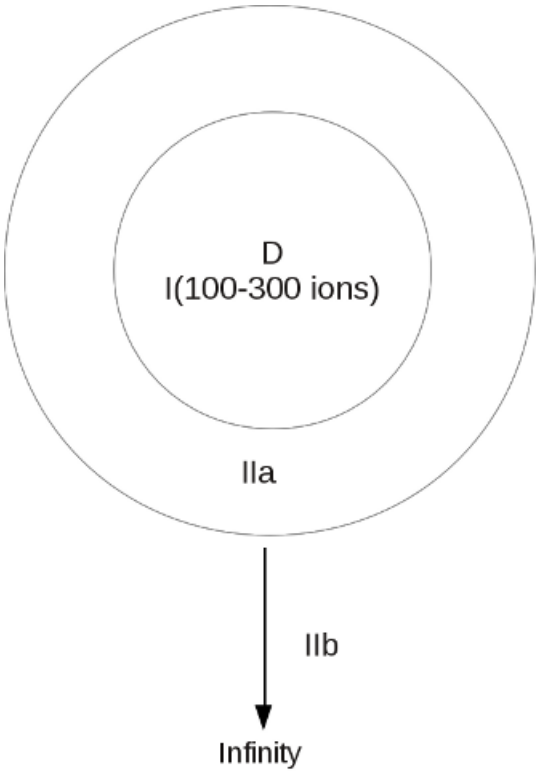

Figure 3.4: Two-region strategy used in defect (D) simulations.

where ε is the dielectric constant of the crystal. Equation (3.42) is strictly applicable to cubic materials. Within the two-region approximation, the energy E_D of the defect formation can be written as,

$$E_D = E_1(x) + E_{I-II}(x,y) = E_y(\mathbf{y}), \tag{3.43}$$

where E_1 is the energy arising solely from interaction of ions within region I i.e self energy of region I, whose coordinates make up the vector x, E_{II} is the self energy of region II for which **y** is the vector of coordinate displacements and E_{I-II} is an interaction energy term. If the displacements y are sufficiently small, then by assuming the validity of harmonic approximation,

$$E_{II} = \frac{1}{2} y.\mathbf{A}.\mathbf{y}, \tag{3.44}$$

where **A** is the force constant matrix. Applying the equilibrium condition to region II, (3.44) becomes,

$$(\frac{\delta E_{I-II}(x,y)}{\delta y})_{y=\vec{y}} = -\mathbf{A}\mathbf{y}. \tag{3.45}$$

Thus, substituting equation (3.45) into equations (3.44) and (3.42) gives,

$$E_D = E_1(x) + E_{I-II}(x,y) - \frac{1}{2}(\frac{\delta E_{I-II}(x,y)}{\delta y}).\mathbf{y}. \tag{3.46}$$

This therefore removes the explicit dependence of E_D on E_{II}, which is convenient. In equation (3.44), $\mathbf{A}^{-1}$ can be equated to $\mathbf{G}^o$, the perfect lattice Green's function for the system. It is worth noting that, the inner region might include a quantum mechanically described species containing a number of variational parameters λ used in optimizing the wave function. Hence, expanding the derivative in equation (3.45) to first order in y gives,

$$-\frac{\delta E_{I-II}}{\delta y} = \mathbf{F}^o(\lambda,x) + \mathbf{F}^1(\lambda,x)\mathbf{y} = \mathbf{A.y} \tag{3.47}$$

Therefore,

$$\mathbf{F}^o(\lambda,x) = [\mathbf{A} - \mathbf{F}^1(\lambda,x)]\mathbf{y} \tag{3.48}$$

and

$$\mathbf{y} = \mathbf{G}\mathbf{F}^o(\lambda,x) \tag{3.49}$$

where

$$\mathbf{G} = [\mathbf{A} - \mathbf{F}^1(\lambda,x)] \tag{3.50}$$

G is now the perturbed Green's function, which allows us to calculate the response of the crystal to the defect (Catlow & Mackrodt, 1982).

CHAPTER FOUR

METHODOLOGY

4.1 Introduction

In this study, bulk and electronic properties as well as properties due to the presence of defects have been studied via *ab-initio* pseudopotential plane wave method with DFT. All calculations in this study were based on DFT as implemented in the Quantum Espresso (Q.E) (Thomas, *et.al*., 1995) suite of computer codes which is a multi-purpose, multi-platform software for *ab-initio* calculations. Q.E stands for Quantum-opEn-Source Package for Research in Electronic Structure, Simulation and Optimization. The code uses plane wave basis sets for the expansion of the electronic wave function, a pseudopotential description of the electron-ion interaction and DFT for description of electron-electron interactions (Giannozzi, *et.al*., 2009). Details of pseudopotentials used in this study are given in Appendix C.

4.2 Electronic and structural Optimization

The most important factors that determine the precision of numerical calculations done in DFT are; type of pseudopotential used, cutoff energy for the plane wave basis set and $k-$points sampling for the Brillouin Zone (BZ) (Frank, *et.al*., 2004). In modelling CsI, starting theoretical values were set at available experimental data (Ashutosh, *et.al*., 2013).

4.2.1 $k-$ points optimization

Brillouin-Zone integrations were performed using the Monkhorst-Pack scheme $k-$ point mesh (Stefano, *et.al*., 2003) . The Monkhorst-Pack scheme ensures that the irreducible part of the BZ is within a mesh of uniformly spaced $k-$ points. To minimize computational time, the cut-off energy was fixed at 25 Ry during the optimization of the $k-$ point mesh. It was evident from Figure 4.1 that CsI has a cubic structure, a = b =c, and therefore $k-$ points were varied from $2\times2\times2$ to $14\times14\times14$, whereby a $6\times6\times6$ grid was found to give the minimum energy (see Figure A.1 in Appendix A) and it was thus

used throughout the subsequent calculations in this work. It was also used to optimize the cut-off energy (E_{cut}) and Volume (V).

4.2.2 Optimization of the plane-wave cut-off energy

The plane-wave cut-off energy was varied from 15 to 60 Ry (see Figure B.3 in Appendix.B). From these values, an optimum value of 45 Ry was chosen, since the energies were well converged when the difference between self consistent steps was less than 10^{-6} Ry.

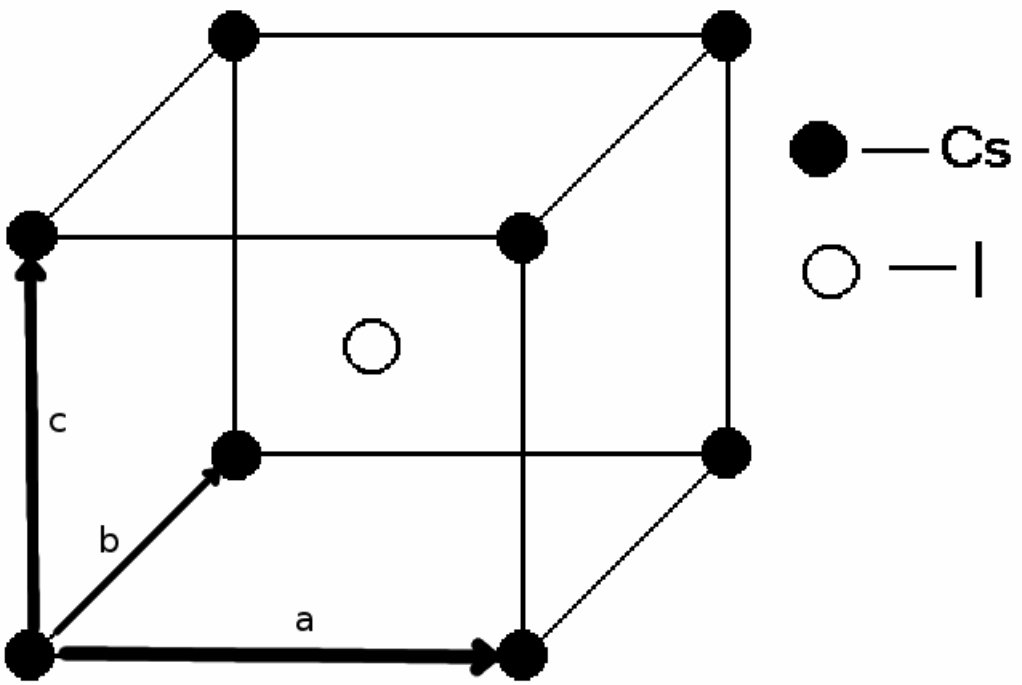

Figure 4.1: Conventional unit cell of Cesium Iodide .

All the calculations reported in this work were carried out at ground state, while most experiments are normally done at slightly higher temperatures and pressures (Jeffrey, *et.al.*, 2004). The lattice constant, a_0, corresponds to the size of a conventional unit cell length at equilibrium volume, V_0, and in this study, a_0 was calculated by minimizing the total energy as a function of the cell volume. The lattice parameter was varied from 7.6 Bohr to 10.8 Bohr in steps of 0.2 Bohr (see Fig. B.2 in Appendix.B). The bulk modulus, B_0, and its pressure derivative, $B_0^{'}$, were obtained by fitting the energy-volume, (E-V), data to the Birch-Murnaghan and Vinet equations of state (Valentín, *et.al.*, 1996).

4.2.3 Size of cells used

The electronic structure representing simple cubic Cesium Iodide was defined by placing a Cesium atom at (0.0,0.0,0.0) and an Iodine atom at (0.50,0.50,0.50) of the lattice parameter as shown in Figure 4.2 . During optimization of CsI, a cell of 8 ($2 \times 2 \times 2$) atoms, and

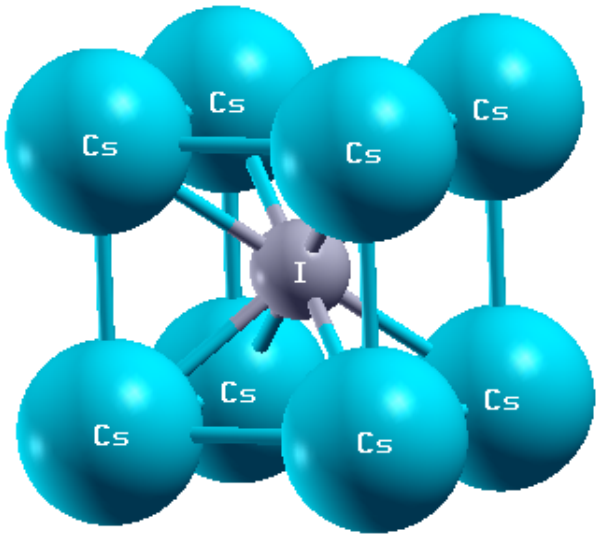

Figure 4.2: Atomic structure of pure Cesium Iodide crystal.

it was used. After optimization a supercell of 128 atoms was constructed which included 64 Cesium atoms and 64 Iodine atoms was used throughout the study. This size was chosen since the defects were well isolated from each other. The defect was introduced to the supercell by either adding atoms (Interstitial) or removing atoms (vacancy). Anionic or cationic migration energies were obtained by moving the atoms at various intervals towards the vacant lattice site in the crystal. The advantage of the supercell model in DFT is that the electronic structure of the unit cell is periodic. All structures were visualized with the graphical visualization code Xcrysden (Anton, 1999).

4.3 Calculation of defect formation energies

4.3.1 Vacancies and Interstitials formation energies

To calculate the formation energy for a single interstitial, E_i^f, the total energy of the relaxed perfect crystal, E_c, was first calculated before introducing an interstitial. After introducing a single interstitial into the relaxed system, the crystal was again relaxed so as to calculate the total energy of the system with an interstitial, E_i. The interstitial formation energy is then given by,

$$E_i^f = E_i - E_c - E_a, \tag{4.1}$$

where E_a is the energy of a free single atom of either Cesium in case of cation or Iodine in case of anion. The energy E_a of a single atom was obtained by placing the atom in a large cubic box of 34.456 Bohr (i.e about 4 times cell lattice constant) in size and relaxing it.

Vacancy formation energy , E_v^f, for a single vacancy for both cation and anion was calculated by removing one atom of Cesium or Iodine and the lattice relaxed upto the set convergence criteria. The vacancy formation energy was calculated by using the expression,

$$E_v^f = E_v - E_c + E_a, \tag{4.2}$$

; where E_v is the relaxed energy of the crystal containing the vacancy.

4.3.2 Frenkel defect formation energies

A Frenkel defect is a neutral defect made up of a paired vacancy and an interstitial (see Figure 4.3)

The formation energy of a frenkel defect, E_F, was calculated as,

$$E_F = E_i + E_v - 2(E_c). \tag{4.3}$$

where E_i is the total energy of the system with an interstitial, E_v is the relaxed energy of the crystal containing the vacancy and E_c is the total energy of the relaxed perfect

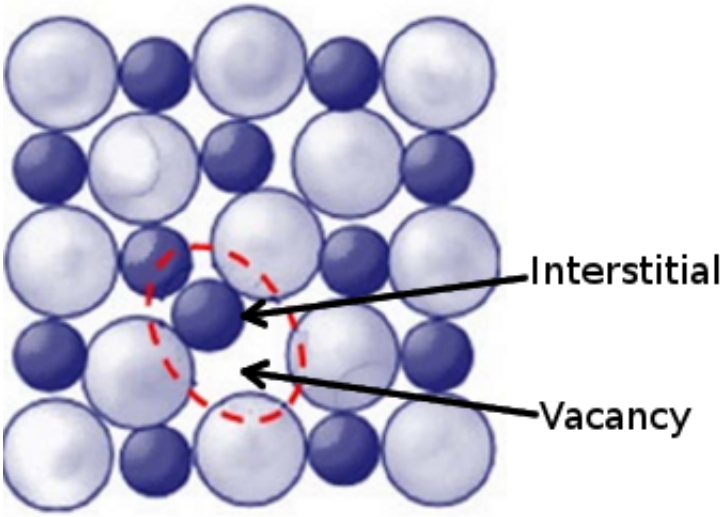

Figure 4.3: A schematic diagram showing a Frenkel defect (Lifshitz & Kosevich, 1966).

crystal. The separation between Frenkel defects are assumed to be infinite such that there is no interaction between them. This separation distance was achieved by calculating both vacancy and interstitial energies separately. Frenkel pair formation energy was also determined at near distances by creating an interstitial and a vacancy close to each other. The defect formation energy was obtained by calculating the energy difference between the energy of the bulk supercell and that of the relaxed supercell containing cation or anion. Thus the Frenkel defect formation energy E_F was obtained from the relation

$$E_F = E_{disp} - E_c, \tag{4.4}$$

where E_{disp} is the energy of the relaxed system when the atom is displaced. Defect concentration was calculated as;

$$\text{Defect concentration} = \frac{\text{No. of defective atom(s)}}{\text{Total no. of atoms in the structure}} \times 100\%. \tag{4.5}$$

4.3.3 Vacancy migration energy

When vacancies migrate in intervals towards a neighbouring site, they must pass through a saddle point. A saddle point is defined as the point where the total energy of the model lattice is at its maximum for a particular migration route; $< 100 >$, , $< 110 >$, and

$< 111 >$. This is given by a relation,

$$E_m^v = E_{i2} - E_{i1}, \tag{4.6}$$

where E_m^v is the energy of vacancy migration, E_{i2} is the energy of atomic interaction in the presence of two vacancies in the ith configuration sphere and the atom located at the saddle point between ith and the $(i-1)$th configuration spheres and E_{i1} is the energy of atomic interaction in the presence of a vacancy in the ith configuration sphere.

CHAPTER FIVE

RESULTS AND DISCUSSION

This chapter presents the results obtained in this work. It includes results on the bulk and electronic properties of CsI, defects and their effects on the band structure of CsI as well as cationic and anionic migration energies in CsI.

5.1 Bulk properties of Cesium Iodide

5.1.1 Equilibrium bulk properties of CsI

Figure 5.1 shows an optimized simple cubic structure of CsI with a Cs and an I atom as the basis.

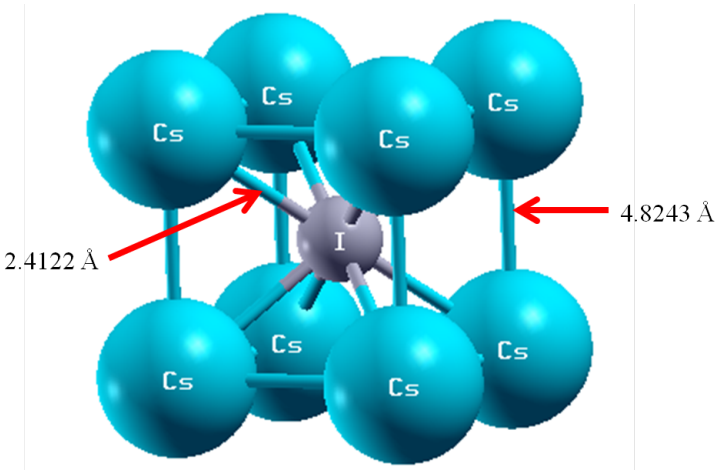

Figure 5.1: Atomic structure of pure Cesium Iodide crystal.

The results obtained from this work were then compared with other theoretical and experimental findings where available. Some of the structural properties of CsI obtained from figure 5.1 include its lattice parameter (a_0), bulk modulus (B_0) and the pressure derivative ($B_0^{'}$) of bulk CsI as well as Cs-Cs (4.8243$\AA$) and Cs-I (2.4122$\AA$) bond lengths. These are summarised in Table 5.2.

From Table 5.2, the structural parameters of CsI obtained in this work were found to vary slightly with experimental values. In particular, the calculated lattice constant, a_0 = 4.551 $\AA$, obtained in this work differed by -0.35% when compared to experimental value of 4.567 $\AA$ (Ribeiro, *et.al.*, 2006) .

Table 5.1: Calculated equilibrium bulk properties of pristine structure of CsI using Birch - Murnagan (B- M) equation of state.

	This study	Experiment[a]	% Dev
a_0 ($\AA$)	4.551	4.567	-0.35
B_0 (GPa)	11.6	11.9	-2.52
$B_0^{'}$	6.30	5.93	+6.24
Cs-Cs	4.8243$\AA$	....	...
Cs-I	2.4122$\AA$	....	.....

[a] (Ribeiro, *et.al*., 2006)

The bulk modulus of 11.6 GPa, calculated in this study differed by -2.52% when compared to experimental value of 11.9 GPa (Ribeiro, *et.al*., 2006), while the calculated pressure derivative, $B_0^{'}$ = 6.30, differed by + 6.24% as compared to experimental value of 5.93 (Ribeiro, *et.al*., 2006). The reduced bulk modulus suggested a slightly softer CsI structure compared to the experimental one.

The calculated bulk values (see Table 5.2) in this study are in close agreement to the experimental values though with some deviations. Such deviations are well known in DFT, and they are attributed mainly to the assumptions made in the theory, since DFT calculations are exact in principle but approximate in practice.

Table 5.2: Calculated properties of defective CsI crystal using Birch - Murnagan (B- M) equation of state.

Defect	B_o(GPa)	$B_o^{\prime}$	Cs-Cs($\AA$)	Cs-I($\AA$)
Cs-interstitial	12.5	5.0	4.4128	1.9919
I-interstitial	12.5	5.0	4.5595	2.2942
Cs-vacancy	12.5	5.0	4.5583	2.2791
I-vacancy	12.5	5.0	4.5874	2.2791
Expt. values	11.9	5.93	-	-

Table 5.2 showed that the bulk modulus increased from 11.9 GPa to 12.5 GPa, which is +5.04% of experimental value and +7.76% of the calculated pristine value for all the defects considered. This increase is attributed to the change in structure within the defective CsI crystal. Similarly, the pressure derivative decreased from 5.93 to 5.0, which is -15.68% of experimental value and -20.63% of the calculated pristine value. This showed a slight disruption of CsI structure upon introduction of defects.

The Cs-Cs bond length decreased from 4.8243 $\mathring{A}$ to 4.307 $\mathring{A}$, which is -10.72% in the case of a Cs-interstitial and the Cs-I bond length also decreased from 2.4122$\mathring{A}$ to 1.387$\mathring{A}$, which is -42.5%. This agreed well with the work of Sung & Sung, (1996) where they established that the bulk modulus increases with decreasing inter atomic distances.

5.2 Electronic properties

5.2.1 Band structure (BS) and projected density of states (PDOS) of pure CsI

Figure 5.2 shows the electronic band gap of pure CsI, which was calculated using 30 k-points sampling of the BZ. A direct band gap of 3.71 eV located at *G* was obtained (Fermi level was put at 0 eV), suggesting that the material is indeed an insulator. This was, however underestimated when compared to the experimental value of 6.2 eV (Ribeiro, *et.al*., 2006), and hence the value obtained in this study has a deviation of about +60% of the experimental value. Several other theoretical calculations have been reported such as in (Ribeiro, *et.al*., 2006) which gave a band gap of 3.91 eV for CsI. This suggests that although the value obtained in this study is underestimated from experiment, it is within the range obtained by other first principle calculations. Figure 5.2 shows the bands superim-

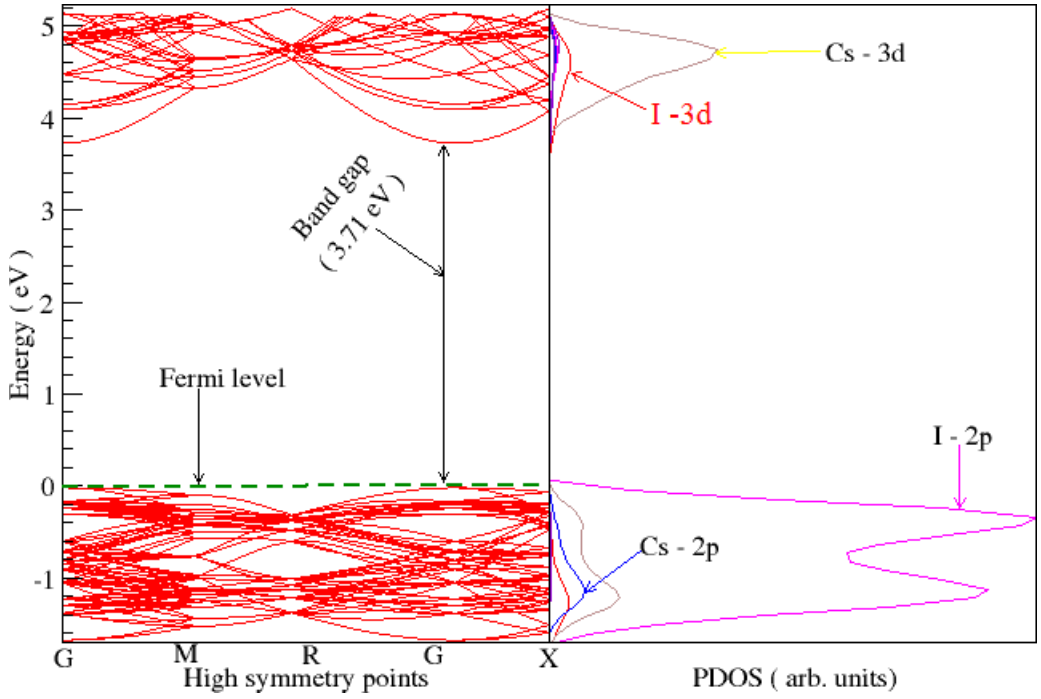

Figure 5.2: Band structure of pure CsI.

posed on the projected density of states for pure CsI. PDOS gives more information on the contribution of each orbital to the excited states as well as to bonding states. From figure 5.2, it is clear that the electronic states of CsI were constituted of an upper valence

band centered between 0 and -1.8 eV and a conduction band of width of 1.44 eV, which is -31.43% of the experimental value (DiStefano & Spicer, 1973). The valence band is dominated by I (2p) and contribution from Cs (2p) states located between -1.2 eV an 0.2 eV. From this study, it is established that the valence band maximum was occupied mainly by I (2p) states and some contribution of Cs (2p) states giving rise to the hybridization of the p-orbitals from the two elements which are responsible for the observed bonding of CsI. The conduction band is characterized mainly by Cs-3d and a little hybridization of I-3d. It is important to point out that zero PDOS for an energy level means that, there are no occupied states.

5.2.2 Density of States (DOS) for pure CsI.

The importance of DOS is that it gives information about the bonding within solids and in classification of materials as either metals, semiconductors or insulators. Metals have no band gap (separation between valence and conduction band), while materials with a large band gap ($\geqslant$ 4 eV) are classified as insulators and semiconductors have a small band gap ($\leq$ 3.4 eV) [John, L., *et.al*., 2009]. DOS for the CsI crystal have been plotted to show the contributions of the atoms on the electronic structure of CsI (Figure 5.2). The plot confirms that CsI is indeed an insulator.

5.3 GW Approximation

Confronted by the band gap underestimation by DFT, GW calculation was performed whereby Bethe salpeter equation(BSE) and Random phase Approximation(RPA) methods were applied to calculate the spectra of CsI. A plot of the intensity versus the energy values is shown in Figure 5.3. The intensity was obtained between 0 and 10 eV. The spectrum in Figure 5.3 shows a sharp rise in intensity resulting in high intensity peaks at 4.2 eV and 5.5 eV from the BSE and RPA methods, respectively. The point at which the spectrum rises sharply indicates the band edge of CsI. This method predicts the band gap of 5.5 eV as compared to LDA method in which the value was obtained as 3.71 eV. This is an improvement by 48.25% from the LDA value though still an underestimation by 11.29% from the experimental value of 6.2 eV. Other theoretical studies obtained the band gap of

4.78 eV and 5.49 eV (Luke & Gao, 2013) (Self-energies calculated band gap) using the same method. Also, Gao, F., *et.al*., (2013) obtained a band gap of 3.15 eV using LDA method as compared to 3.71 eV obtained in this study.

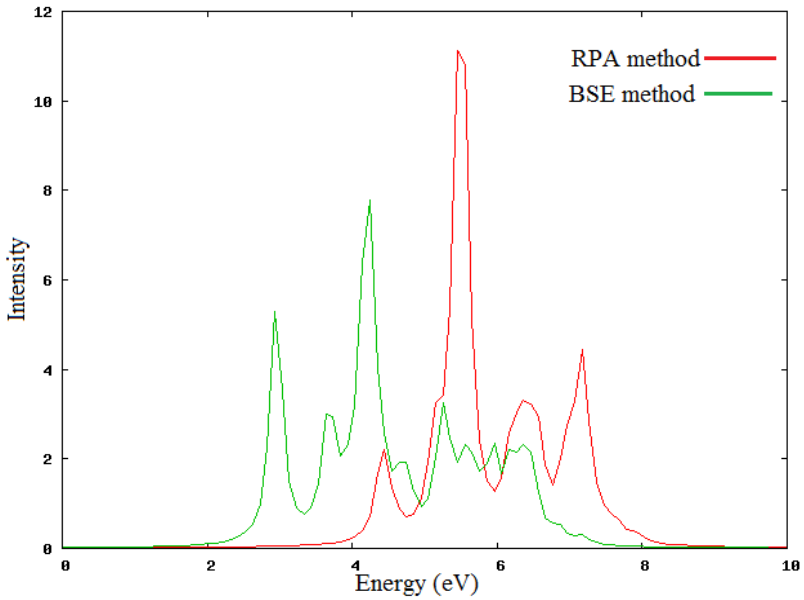

Figure 5.3: A plot of intensity versus energy spectra of bulk CsI.

Table 5.3 shows a comparison of electronic properties of pristine CsI obtained in this study and other theoretical calculations as well as some experimental work .

Table 5.3: Energies of selected transitions between the highest valence band and lowest conduction band.

Transition	Bandgap (eV)			
	This study	GW(1)[b]	GW(2)[b]	Experiment
$\Gamma \rightarrow \Gamma$	5.5	4.78	5.49	6.1[c], 6.3[d], 6.37[e], 6.0[f]
$M \rightarrow \Gamma$	4.2	4.74	5.44	

[b] (Luke & Gao, 2013), [c](Yun-Ching, *et.al*., 2013), [d](James, *et.al*., 1984), [e] (Lushchik, *et.al*., 1996) and [f] (James, *et.al*., 2003).

5.4 Band structure (BS) and Projected Density of states (PDOS) of defective CsI.

5.4.1 Vacancy defects

In this study, vacancies were created by removing either Cesium or iodine atoms from the crystal lattice, giving rise to a defect concentration level of $\approx 0.78\%$. The modeled crystal was then used to calculate BS and DOS as well as the PDOS of CsI with the respective vacancies. Figures 5.4 and 5.5 shows the PDOS and BS of CsI structure with Cesium and

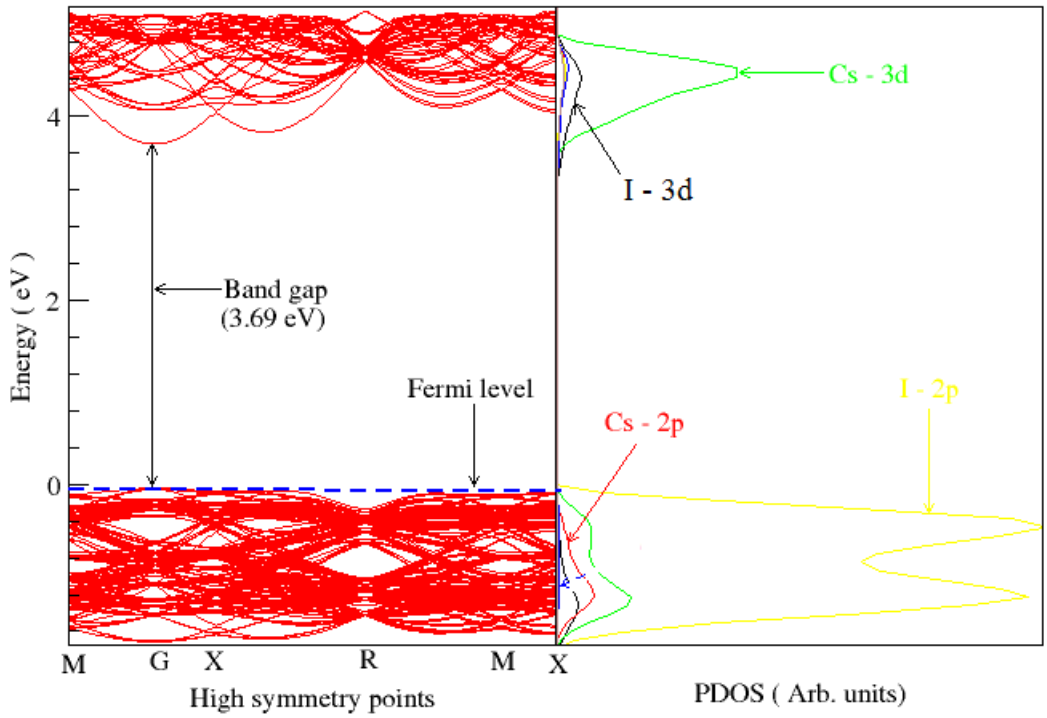

Figure 5.4: Electronic band structure of CsI with a Cesium vacancy.

Iodine vacancies, respectively. The band structure was plotted along the high symmetry path $M-\Gamma-X-R-M-X$ in both structures.

Both the PDOS and BS plots (figure 5.4) showed that the electronic states of the structure with Cesium vacancy were constituted of a valence band of 1.69 eV in width and a narrow conduction band of 0.82 eV. The structure was found to have a direct band gap of 3.69 eV located at G showing an insignificant downward bending of the conduction band edge by 0.02 eV. Similarly, the PDOS and BS plots (figure 5.5) of the structure with

iodine vacancies shows that the structure is constituted of a valence band of 1.71 eV in width and a narrower conduction band of 0.80 eV. The structure was also found to have an insignificant downward bending of the conduction band minimum by 0.04 eV resulting to a direct band gap of 3.67 eV located also along G direction. No formation of defect states was observed due to Cesium and Iodine defects. The Fermi level appear to have dropped from 0.12 eV to -0.16 eV and -0.13 eV due to the presence of Cesium vacancy and Iodine vacancy, respectively, suggesting that the defective crystals have acceptor-like behaviour.

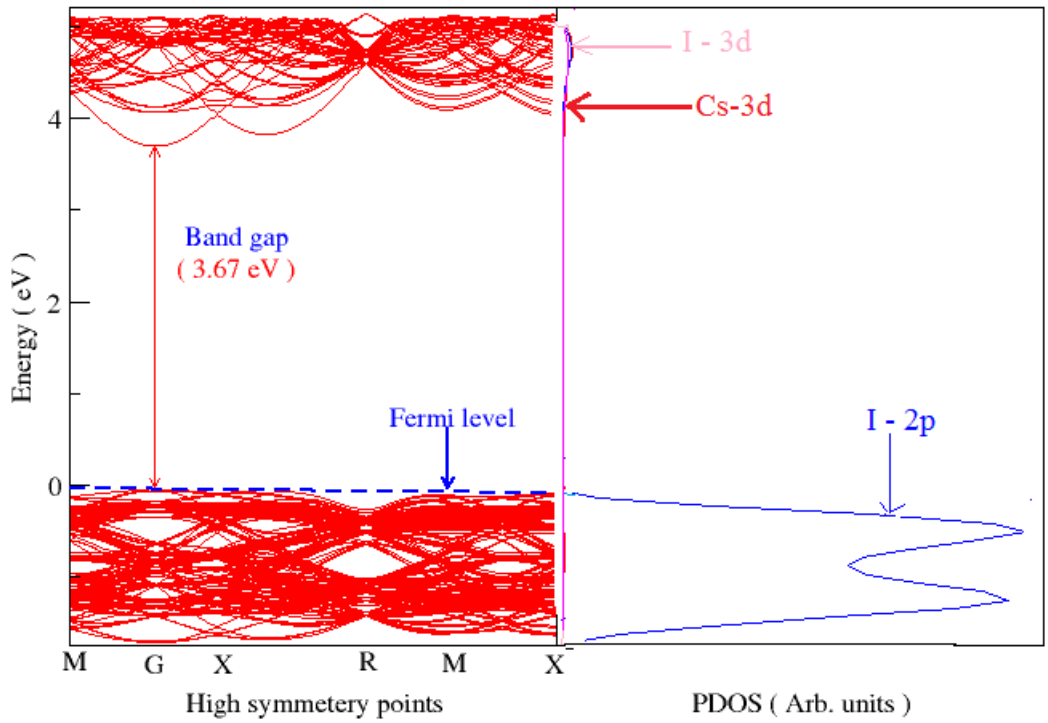

Figure 5.5: Electronic band structure of CsI with an Iodine vacancy.

5.4.2 Frenkel defects

Frenkel defects were created by displacing either a Cesium or Iodine atom by 6.8375 $\AA$ and 3.1168 $\AA$, respectively, within the CsI. Figures 5.6 and 5.7 shows displaced Cesium and Iodine atoms, respectively, within the supercells, to form Frenkel defects.

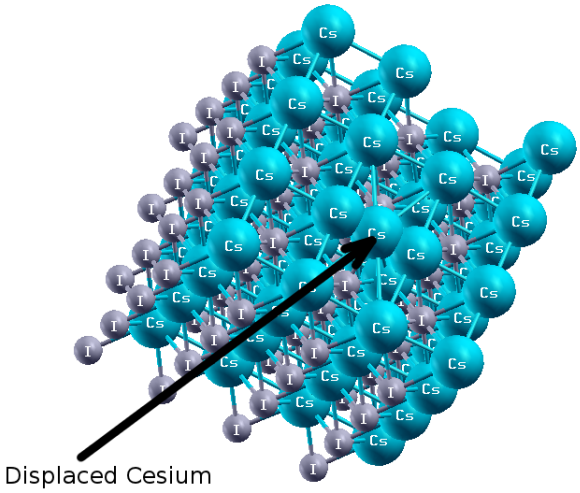

Figure 5.6: A super cell of CsI with a cesium (Cs) atom interstitial.

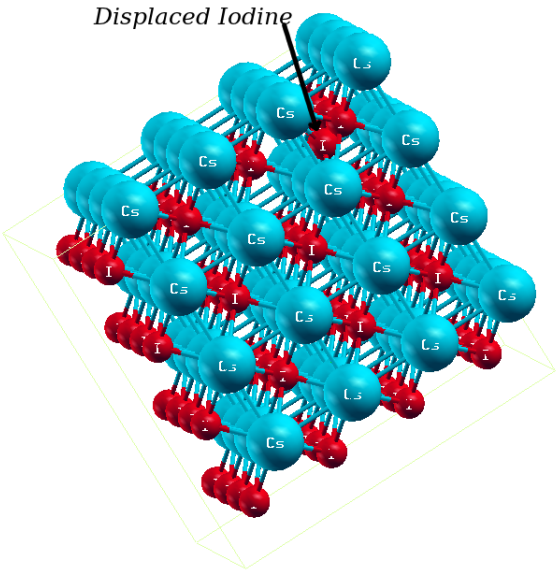

Figure 5.7: A super cell of CsI with an iodine (I) atom interstitial.

Following these displacements and optimization of the structure, the bond lengths were found to decrease from their bulk positions in the pure crystal. Table 5.4 shows the calculated bond length of Cs-Cs and Cs-I after displacement of Cesium and Iodine (Frenkel defects), respectively. In both cation and anion Frenkel defects, the bond lengths

Table 5.4: Calculated DFT-GGA bond lengths in CsI around the Frenkel defect.

Bond	**Before displacement** ($\AA$)	**After displacement** ($\AA$)
Cs-Cs	4.8243	1.2061
Cs-I	2.4122	0.7628
I-I	4.5583	2.279

were found to contract significantly around the defect site. When Cesium atom was displaced from the lattice site, the Cesium atoms came closer towards each other from 4.8243 $\AA$ to 1.2061 $\AA$ while displacing Iodine was found to reduce the bond length from 2.4122 $\AA$ to 0.7628 $\AA$. From these results, it can be postulated that both Schottky and Frenkel

defects affected the structure of CsI with the latter affecting it the most.

5.5 Formation energies

The defective crystals with displaced atoms were used to calculate cationic and anionic Frenkel pair formation energies at infinite distances as shown in Table 5.5. All values of energies are given per formula unit in the structure. The general principle is that the lesser

Table 5.5: Defect pair formation energy (eV) for cation and anion per formula unit in Cesium Iodide.

Method	Cation Frenkel	Anion Frenkel
This study (Infinite distances)	0.21	0.16
Experiment[b] (Infinite distances)	0.56	0.32

[b] (Kun-Dar *et.al*., 2008)

the energy, the easier it takes to form such a defect. Cation Frenkel formation energy was calculated as 0.21 eV and the Anion Frenkel formation energy was found to be 0.16 eV. Due to the low formation energy of anion Frenkel defect, this study suggests that anion Frenkel defect is easily formed as compared to cation Frenkel defect. To compare the formation energies of vacancies and interstitials, the cationic and anionic formation energies were calculated using equations (4.1) – (4.4) in section 4.3 and the results shown in Table 5.6.

Table 5.6: Defect formation energy(eV) for cation and anion in Cesium Iodide.

	Interstitial	Vacancy
Cs	0.4325	0.25
I	0.30	0.16

From this table, a Cesium interstitial was found to be formed with an energy of 0.4325 eV as compared to a Cesium vacancy whose formation is 0.25 eV. This shows that it is not easy to displace a Cesium atom from its lattice site within CsI but it is easier to remove a Cs atom inspite of its large size. This study also established that Iodine interstitial can be formed with an energy of 0.30 eV while an Iodine vacancy can be formed with an energy of 0.16 eV. Thus, it is also easier to form an Iodine vacancy than an Iodine interstitial . Comparing the formation energies of Cesium and Iodine interstitials, it was found that

it was much easier to form an iodine interstitial than the Cesium interstitial. Further, comparing the Cesium and Iodine vacancies, this study found that it is easier to form an Iodine vacancy than a Cesium one by about 0.09 eV. This showed that vacancies can be easily formed than their counterpart interstitials. It is then concluded that lighter atoms are likely to occupy non-lattice site than heavier atoms. These findings are comparable to atomic weights of Cesium and iodine which are 132.9055 amu and 126.9045 amu, respectively. Generally, it appears that it is easier to form vacancies in CsI than creating interstitials in it, a process that may not be easy due to the high energy required to achieve this.

5.6 Defect migration

The cationic migration path was studied by removing a neutral Cesium atom in a crystal lattice site to create a vacancy. Similarly an anionic migration path was studied by removing a neutral Iodine atom in a crystal lattice site to create a vacancy. Both vacancies were created by removing atoms in the crystal atomic sites of the modeled structure. The sites along the migration path were changed in intervals of 0.05 $\AA$ to the next nearest neighbours as they pass through the saddle point.

5.6.1 Cationic migration path

As mentioned earlier, the Cesium vacant positions were approached by another Cesium atom from a different crystal lattice site in steps of 0.05 $\AA$. The atom was allowed to migrate in three different directions; $< 100 >, < 110 >$ and $< 111 >$ (see figures 5.8, 5.9 and 5.10, respectively).

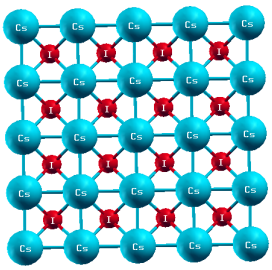

Figure 5.8: $< 100 >$ **Direction.**

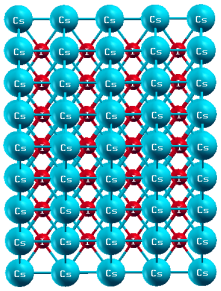

Figure 5.9: $< 110 >$ **Direction.**

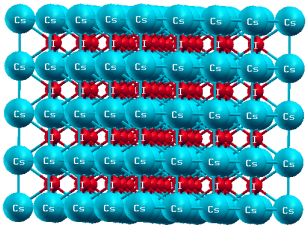

Figure 5.10: $< 111 >$ **Direction.**

Figure 5.11 shows migration energies as a function of migration path in the three different low index directions; $< 100 >, < 110 >$ and $< 111 >$ of CsI. The Cesium atom was found to migrate along the $< 100 >$ direction with saddle point energy of -1.5254 eV, along the $< 110 >$ direction with a saddle point energy of -1.5253 eV and -1.5252 eV along the $< 111 >$ direction (see Appendix D.1). This showed that Cesium atom migrated with the least amount of energy along $< 100 >$ direction. This direction was favoured due to the fact that the $< 100 >$ direction has more large open channels to accommodate the migration of the large Cesium atom, unlike the other directions.

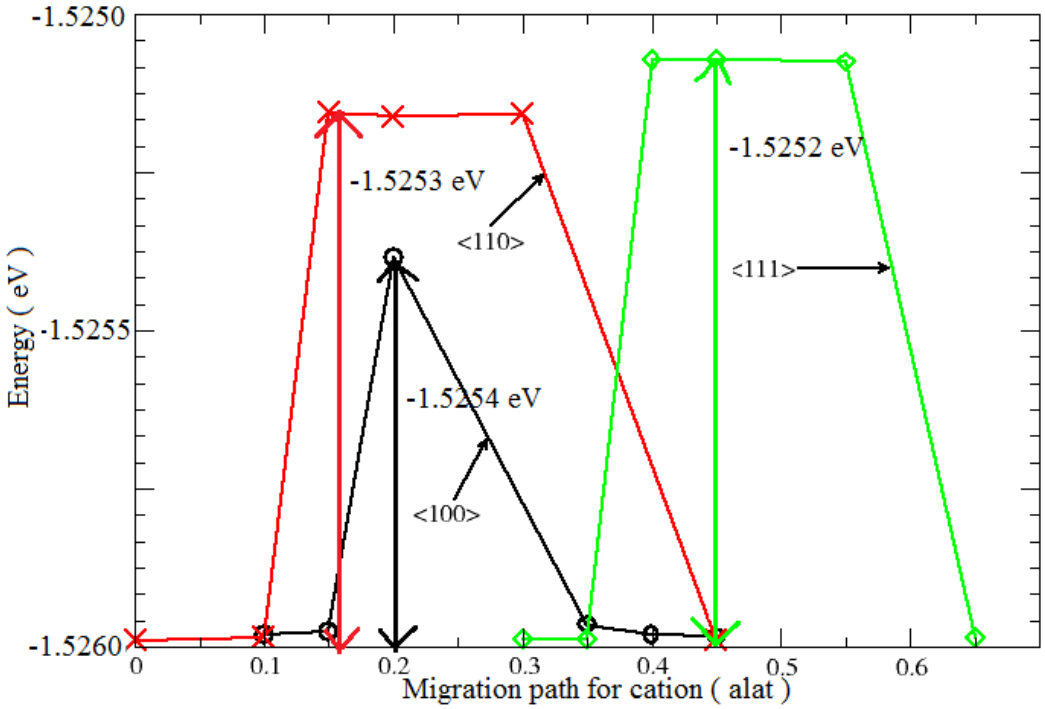

Figure 5.11: Migration path of Cesium ion along the three low index directions.

5.6.2 Anionic migration path

For the case of anionic migrtation the Iodine vacant position was approached by another Iodine atom in a different crystal site in steps of 0.05 $\AA$, just like in the case of the Cesium atom. The Iodine atom was also allowed to migrate in three different directions;$< 100 >$,$< 110 >$ and $< 111 >$. Figure 5.12 shows migration paths along the three low index directions. This study establishes that the Iodine atom migrated with saddle point energy of -1.5050 eV along the $< 100 >$ direction, -1.5048 eV along $< 110 >$ direction and -1.5049 eV along the $< 111 >$ direction (see Appendix D.2). When these values of saddle point ,S , energies were compared, it was found that the Iodine atom preferred to migrate along the $< 100 >$ direction, just as was the case with the Cesium atom. When the migration energies of the two ions, that is, Cs^{+} (ionic radius of 1.81Å) and I^{-} (ionic radius of 2.06 Å) are compared, it was found that the barrier of migration of the Cesium ion was lower at -1.5254 eV compared to that of Iodine at -1.5050 eV along the $< 100 >$ and $< 100 >$directions, respectively.

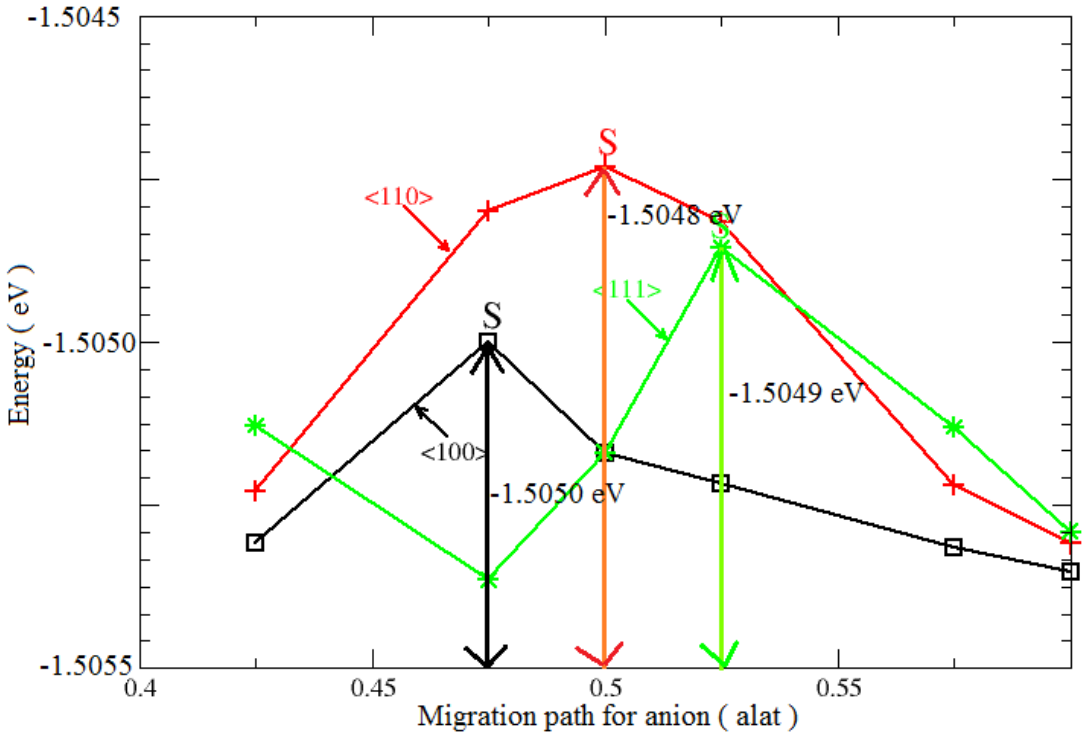

Figure 5.12: Migration path of Iodine ion along the three low index directions.

CHAPTER SIX

CONCLUSION AND RECOMMENDATION

6.1 Conclusion

This study has considered equilibrium bulk properties, electronic properties, defect formation and their migration energies in CsI. The lattice parameter of CsI was found to be 4.551 $\AA$ (using DFT) as compared to an experimental value of 4.567 $\AA$ .The bulk modulus (B_0) was calculated as 11.6 GPa for pure CsI as compared to experimental value of 11.9 GPa. The pressure derivative ($B_0^{'}$) was computed to a value of 6.30 as compared to an experimental value of 5.93. These values showed close agreement to experimental data available. After adding the defects, these values were found to change quite significantly. In particular, the bulk modulus increased by 5.04% upon the introduction of the various point defects while the pressure derivative decreased by 25.40% from that of the pristine structure. The Frenkel defects resulted in Cs-Cs bond length change from 4.8243 $\AA$ to 1.2061 $\AA$ and Cs-I bond length change from 2.4122 $\AA$ to 0.7628 $\AA$.

From the electronic properties of CsI, the calculated band gap of pure CsI using DFT was 3.71 eV which was 40 % below the experimental value of 6.2 eV as DFT normally underestimates the fundamental gap. The GW approximation method predicted a much wider band gap of 5.5 eV as compared to LDA method by a value of 1.79 eV. Since the experimental value was 6.2 eV, it is concluded that GW method is better than LDA method in approximating band gaps of materials. The defective CsI with Cs vacancy and I vacancy led to a very small downward bending of the CB edge leading to observed reduced band gap of 3.69 eV and 3.67 eV, respectively.

Also, from the results of defect formation energies it was observed that cesium interstitial was formed with an energy of 0.4325 eV while iodine interstitial was formed with an energy of 0.30 eV. The study therefore showed that it is easier to form iodine interstitial than the one of cesium. Cesium vacancy was formed with an energy of 0.25 eV while iodine vacancy was formed with an energy of 0.16 eV. This showed that iodine vacancy was easier to form as compared to cesium vacancy, probably due to the difference in their

sizes.

The migration of both cesium and iodine atoms in CsI was found to occur mostly along the $< 100 >$ direction due to large open channels to accommodate the migration of both atoms. Cesium and Iodine migrated with least energies of -1.5254 eV and -1.5050 eV along the $< 100 >$ direction, respectively. This showed that the large size of Iodine prevented it from diffusing easily along the three low index directions.

In general, the various defects in CsI were established to affect both the structural and electronic properties of CsI. Both interstitials and vacancies increased the bulk modulus from 11.9 GPa to 12.5 GPa. Similarly, both vacancies and interstitials decreased the pressure derivative from 5.93 to 5.00. Cesium and Iodine vacancies reduced the band gap from 3.71 eV to 3.69 eV and 3.67 eV, respectively. The calculated formation energies of Cesium and Iodine showed that Iodine interstitial and its vacancy were easier to form than Cesium interstitial and its vacancy. Last but not least, the calculated migration energies showed that both Cesium and Iodine preferred to migrate along the $< 100 >$ direction.

6.2 Recommendation

The study has dealt with defects involving only a few atoms and it is therefore recommended that the study be extended to include multi-atom defects. There is also need to study the effect of simultaneous point defects in CsI crystal which was not addressed here. It is further recommended that study of the migration of atoms using the nudged elastic band calculation method be carried out. Further studies on point defects in CsI should use DFT + U, in order to determine the band gaps more precisely.

LIST OF REFERENCES

Alexander, K.(2014). On the Hartree-Fock dynamics in wave-matrix picture. *arXiv preprint arXiv*,1407,5208.

Amolo, GO., Erasmus, RM., Comins, JD. & Derry, TE. (2006). Raman and optical absorption studies of proton bombarded CsI. *Nuclear Instruments and Methods in Physics Research Section B: Beam Interactions with Materials and Atoms*, 250(1), 359-362.

Andres, L. & Eva, N. (2006). The orthogonal tilt reconstruction method: an approach to generating single-class volumes with no missing cone for *ab initio* reconstruction of asymmetric particles. *Journal of structural biology*,153(3),284-299.

Anton, K. (1999). XCrySDena new program for displaying crystalline structures and electron densities. *Journal of Molecular Graphics and Modelling*, 17(3), 176-179.

Arthur, M.(2002). Redistribution of point defects in the crystalline lattice of a semiconductor in an inhomogeneous temperature field. *Defect and Diffusion Forum*,210,89-102.

Ashutosh, D., Knapp, R. & Pillai, M. (2013). Industrial radionuclide generators: a potential step towards accelerating radiotracer investigations in industry. *RSC Advances*, 3(35), 14890-14909.

Bernard, V. (1947). The nucleation of ice formation by silver iodide. *Journal of applied physics*, 18(7), 593-595.

Bing, H., Liang, H., Ni, H., Su, Q., Yang, G., Shi, J., *et.al.* (2009). Intense red light emission of Eu 3+-doped LiGd (PO 3) 4 for mercury-free lamps and plasma display panels application. *Optics express*, 17(9), 7138-7144.

Butman, M., Kudin, L., Smirnov, A. & Munir, Z. (2000). Mass spectrometric study of the molecular and ionic sublimation of cesium iodide single crystals. *International Journal of Mass Spectrometry*, 202(1), 121-137.

Çağlar Ö, G., Meyer, J., Erni, R., Rossell, M., Kisielowski, C., Yang, Li., *et.al.* (2009). Graphene at the edge: stability and dynamics. *Science*, 323(5922), 1705-1708.

Carlos, O. & Carl, C. (2007). Secondary electron cascade dynamics in KI and CsI. *The Journal of Physical Chemistry C*, 111(46), 17442-17447.

Catlow, C. & Mackrodt, W. (1982). Theory of simulation methods for lattice and defect energy calculations in crystals. *Computer simulation of solids*, 1-20.

Cawkwell, M. & Niklasson, A. (2012). Energy conserving, linear scaling Born-Oppenheimer molecular dynamics. *The Journal of chemical physics*, 137(13), 134105.

Damian, J., Peng, K., Feinstein, D. & Kilian, A.(2001). Diversity arrays: a solid state technology for sequence information independent genotyping. *Nucleic acids research*, 29(4), 25.

David, K., Flach, S. & Kivshar, Y. (2004). Localizing energy through nonlinearity and discreteness. *Physics Today*, 57(1), 43-49.

David, V. & King-Smith, R. (1998). Electronic polarization in the ultrasoft pseudopotential formalism. *arXiv preprint cond-mat/9801177*.

DiStefano, TH. & Spicer, WE. (1973). Photoemission from CsI: experiment. *Physical Review B*, 7(4), 1554.

Eberhard, G. & Dreizler, R. (2013). *Density functional*. 337.

Fabien, F. & Blaha, P. (2009). Accurate band gaps of semiconductors and insulators with a semilocal exchange-correlation potential. *Physical Review Letters*, 102(22), 226401.

Frank, V., Porras, D. & Cirac, J. (2004). Density matrix renormalization group and periodic boundary conditions: a quantum information perspective. *Physical Review Letters*, 93(22), 227205.

Furqan, A., Choudhury, N., Dutta, N., Brito e Abreu, S., Zannettino, A., Duncan, E., *et.al*. (2014). Interaction of Platelets with Poly (vinylidene fluoride-co-hexafluoropropylene) Electrospun Surfaces. *Biomacromolecules*, 15(3), 744-755.

Georg, K. & Joubert, D. (1999). From ultrasoft pseudopotentials to the projector augmented-wave method. *Physical Review B*, 59(3), 1758.

George, B., Andreas, G., Kresse, G. & Alavi, A.(2013). Towards an exact description of electronic wavefunctions in real solids. *Nature*, 493(7432), 365-370.

Glenn, F. (2010). *Radiation detection and measurement*. John Wiley & Sons.

Graeme, H., Gísli, J. & Hannes, J. (2002). Methods for finding saddle points and minimum energy paths. *Theoretical Methods in Condensed Phase Chemistry*, 269-302.

Hagen, G., Hjorth-Jensen, M. & Michel, N. (2006). Gamow shell model and realistic nucleon-nucleon interactions. *Physical Review C*, 73(6), 064307.

Harry, L. & Bishop, S. (2011). Point defects in oxides: tailoring materials through defect engineering. *Annual Review of Materials Research*, 41, 369-398.

Hirai, T., Ichimura, N., Hashimoto, S., Nakayama, T., Yoshimura, Y., Iwasaki, H., *et.al*. (1998). Optical and x-ray studies of thin mixed crystals of NaCl-typed RbI and CsCl-typed CsI. *Journal of Chemical Physics*, 109(5), 1863-1866.

Hubbell, JH. & Seltzer, SM. (2004). Tables of X-ray mass attenuation coefficients and mass energy-absorption coefficients. *National Institute of Standards and Technology, Gaithersburg, MD*, 1.4.

Istratov, A. & Weber, E. (2005). Structural, elemental, and chemical complex defects in silicon and their impact on silicon devices. *Electrochemical Society Interface*, 14(1), 34-36.

Itaru, S., Kudo, H. & Tsuda, S. (2011). Removal efficiency of water purifier and adsorbent for iodine, cesium, strontium, barium and zirconium in drinking water. *The Journal of toxicological sciences*, 36(6), 829-834.

James, P., Nagel, S., & Ramakrishnan, T. (1984). Dipolar reorientation and phase transitions in mixed alkali-halide-alkali-cyanide crystals. *Physical review letters*, 53(26), 2489.

James, T., Samei, E., Chotas, H., Warp, R., Baydush, A., Floyd Jr, C., *et.al*. (2003). Chest radiography: optimization of X-ray spectrum for cesium iodide–amorphous silicon flat-panel detector 1. *Radiology*, 226(1), 221-230.

Janghwan, C., Lim, S., Choi, C.,Moon-Hyun C. & Park, N. (2009). Inaccuracy of density functional theory calculations for dihydrogen binding energetics onto Ca cation centers. *Physical review letters*, 103(21), 216102.

Jan, H. (2001). Intermolecular exchange-induction and charge transfer: Derivation of approximate formulas using nonorthogonal localized molecular orbitals. *The Journal of Chemical Physics*, 114(20), 8775-8783.

Jan, M. (2004). Study of the nucleation and growth of cesium iodide and cesium chloride on cesium iodide substrates. *Journal of Research (Science)*, 15(4), 461-469.

Jeffrey, C., Schwegler, E., Draeger, E., Gygi, F. & Galli, G. (2004). Towards an assessment of the accuracy of density functional theory for first principles simulations of water. *The Journal of chemical physics*, 120(1), 300-311.

Jianmin, T., Perdew, J., Staroverov, V. & Scuseria, G. (2003). Climbing the density functional ladder: Nonempirical meta–generalized gradient approximation designed for molecules and solids. *Physical Review Letters*, 91(14), 146401.

Johnson, R., Dienes, G. & Damask, A. (1964). Calculations of the Energy and Migration Characteristics of Carbon and Nitrogen in α-Iron and Vanadium. *Acta Metallurgica*, 12(11), 1215-1224.

John, L., Dabbs, J. & Levine, N. (1973). Scintillator handbook with emphasis on cesium iodide.

John, P., Burke, K. & Wang, Y. (1996). Generalized gradient approximation for the exchange-correlation hole of a many-electron system. *Physical Review B*, 54(23), 16533.

John, P. & Zunger, A. (1981). Self-interaction correction to density-functional approximations for many-electron systems. *Physical Review B*, 23(10), 5048.

Kimerling, L. (1978). Recombination enhanced defect reactions. *Solid-State Electronics*, 21(11), 1391-1401.

Korir, K., Amolo, GO., Makau, NW. & Joubert, DP. (2011). First-principle calculations of the bulk properties of 4d transition metal carbides and nitrides in the rocksalt, zincblende and wurtzite structures. *Diamond and Related Materials*, 20(2), 157-164.

Kosloff, R. & Tal-Ezer, H. (1986). A direct relaxation method for calculating eigenfunctions and eigenvalues of the Schrödinger equation on a grid. *Chemical Physics Letters*, 127(3), 223-230.

Kun-Dar, L., Xiao, H. & Wang, L. (2008). Computer simulation study of defect formation and migration energy in calcium fluoride. *Nuclear Instruments and Methods in Physics Research Section B: Beam Interactions with Materials and Atoms*, 266(12), 2698-2701.

Kurt, E., Kotomin, E. & Uberuaga, B. (2007). *Radiation effects in solids*. 235. Springer

Science & Business Media.

Kurt, L. (1953). Space-charge layer and distribution of lattice defects at the surface of ionic crystals. *The Journal of Chemical Physics*, 21(7), 1123-1128.

Lidiard, A. & McKee, R. (1980). Point defects in silver halides. Kinetics and thermodynamics of the migration of interstitial defects. *Le Journal de Physique Colloques*, 41(C6), C6-91.

Lifshitz, I. & Kosevich, A. (1966). The dynamics of a crystal lattice with defects. *Reports on Progress in Physics*, 29(1), 217.

Lindsey, J. & Wales, D. (1999). Defect migration in crystalline silicon. *Physical Review B*, 59(6), 3969.

Luke, W. & Gao, F. (2013). Excited state electronic properties of sodium iodide and cesium iodide. *Journal of Luminescence*, 137, 121-131.

Lushchik, A., Feldbach, E., Kink, R., Lushchik, Ch., Kirm, M. & Martinson, I. (1996). Secondary excitons in alkali halide crystals. *Physical Review B*, 53(9), 5379.

Martin, S. (2005). Flat detectors and their clinical applications. *European radiology*, 15(9), 1934-1947.

Mary, A., Martins, K. & Herbert, J. (2009). A long-range-corrected density functional that performs well for both ground-state properties and time-dependent density functional theory excitation energies, including charge-transfer excited states. *The Journal of chemical physics*, 130(5), 054112.

Mauricio, C., Bubin, S. & Adamowicz, L. (2003). Non-Born–Oppenheimer calculations of atoms and molecules. *Physical Chemistry Chemical Physics*, 5(8), 1491-1501.

Milman, V,. Winkler, B., White, JA., Pickard, CJ., Payne, MC., Akhmatskaya, EV., et.al. (2000). Electronic structure, properties, and phase stability of inorganic crystals: A pseudopotential plane-wave study. *International Journal of Quantum Chemistry*, 77(5), 895-910.

Mueni, M. (2014). *Structural and electronic properties of TiO2, Cr: TiO2 AND Nb: TiO2 using density fuctional theory*. Unpublished doctoral dissertation. University of Free state, Johannesburg.

Nagarkar, VV., Gupta, TK., Miller, SR., Klugerman, Y., Squillante, MR. & Entine, G. (1998). Structured CsI (Tl) scintillators for X-ray imaging applications. *Nuclear Science, IEEE Transactions on*, 45(3), 492-496.

Paul, E., Träskelin, P. & Albe, K. (2013). Formation and switching of defect dipoles in acceptor-doped lead titanate: A kinetic model based on first-principles calculations. *Physical Review B*, 88(2), 024107.

Paul, G., Baroni, S., Bonini, N., Calandra, M., Car, R., Cavazzoni, C., et.al. (2009). QUANTUM ESPRESSO: a modular and open-source software project for quantum simulations of materials. *Journal of Physics: Condensed Matter*, 21(39), 395502.

Peterson, K. (2003). Systematically convergent basis sets with relativistic pseudopotentials. I. Correlation consistent basis sets for the post-d group 13–15 elements. *The Journal of chemical physics*, 119(21), 11099-11112.

Ping, N., Pilati, S., Troyer, M. & Dai, X. (2012). Density functional theory for atomic Fermi gases. *Nature Physics*, 8(8), 601-605.

Prasad, R. & Bansil, A. (1980). Special directions for Brillouin-zone integration: application to density-of-states calculations. *Physical Review B*, 21(2), 496.

Ribeiro, R. et.al. (2006). Ab initio study of CsI and its surface. *Physical Review B*, 74(3), 035430.

Rihua, M. Zhang, L. & Ren-Yuan, Z. (2007). Optical and scintillation properties of inorganic scintillators in high energy physics. *Nuclear Science Symposium Conference Record, 2007. NSS'07. IEEE*, 3, 2285-2291.

Sandro, S., Giannozzi, P., Cavazzoni, C., de Gironcoli, S., Pasquarello, A. & Baroni, S. (2005). First-principles codes for computational crystallography in the Quantum-ESPRESSO package. *Zeitschrift für Kristallographie-Crystalline Materials*, 220(5/6), 574-579.

Scott, G., Meredig, B., Kirklin, S., Saal, J. & Wolverton, C. (2013). Approaching chemical accuracy with density functional calculations: Diatomic energy corrections. *Physical Review B*, 87(7), 075150.

Shiyou, C., Ji-Hui, Y., Gong, X., Walsh, A. & Su-Huai, W. (2010). Intrinsic point defects and complexes in the quaternary kesterite semiconductor Cu 2 ZnSnS 4. *Physical Review B*, 81(24), 245204.

Simone, P., Lazzeri, M., Casiraghi, C., Novoselov, K., Geim, A., Ferrari, A., *et.al*. (2007). Breakdown of the adiabatic Born–Oppenheimer approximation in graphene. *Nature materials*, 6(3), 198-201.

Stefano, C., Morgan, D., Persson, K., Rodgers, J. & Ceder, G. (2003). Predicting crystal structures with data mining of quantum calculations. *Physical review letters*, 91(13), 135503.

Steven, J. (1998). Scintillator phosphors for medical imaging. *Interface-Electrochemical Society*, 7(2), 34-39.

Stig, L. & March, N. (2013). *Theory of the inhomogeneous electron gas*. Springer Science & Business Media.

Sung, C. & Sung M. (1996). Carbon nitride and other speculative superhard materials. *Chemistry and physics*, 43(1), 1-18.

Taedaehyeong, E., Hyung-Kyu, L., Goddard III, W. & Kim, H. (2014). First-Principles Study of Iron Oxide Polytypes: Comparison of GGA+ U and Hybrid Functional Method. *The Journal of Physical Chemistry C*, 119(1), 556-562.

Thomas, V., Martin, R., & Hay, P. (1995). Effective core potentials for DFT calculations. *The Journal of Physical Chemistry*, 99(47), 17085-17087.

Valentín, B., Taravillo, M., Cáceres, M. & Núñez, J. (1996). Universal features of the equation of state of solids from a pseudospinodal hypothesis. *Physical Review B*, 53(9), 5252.

Vladimir, N. (2007). Optical & scintillation properties of nonmetals: inorganic scintillators for radiation detectors. *Radiation Effects in Solids*, 233-257.

Walter, K. (1999). Nobel Lecture: Electronic structure of matterwave functions and density functionals. *Reviews of Modern Physics*, 71(5), 1253.

Wei,Z., Goran, R. & Rowlands, J (2004). X-ray imaging performance of structured cesium iodide scintillators.*Medical physics*,31(9),2594-2605.

Wheeler, P. (1923). Precision measurements of crystals of the alkali halides. *Physical Review*, 21(2), 143.

William, D. & Rethwisch, D. (2007). *Materials science and engineering: an introduction*(7). Wiley New York.

William, H & Stoneham, A. (2004). *Defects and defect processes in nonmetallic solids*. Courier Corporation.

Xiaofang, W., Krishnan, M., Saleh, N., Wang, H. & Umstadter, D. (2000). Electron acceleration and the propagation of ultrashort high-intensity laser pulses in plasmas. *Physical review letters*, 84(23), 5324.

Yang, L., Cheol-Hwan, P., Young-Woo, S., Cohen, M. & Louie, S. (2007). Quasiparticle energies and band gaps in graphene nanoribbons. *Physical Review Letters*, 99(18), 186801.

Yeong, E. (2014). Purdue Nuclear and Many-Body Theory Group. 5.

Ying, X., John, S., Oganov, A., Cui, T., Wang, H., Ma, Y., *et.al*. (2009). Superconducting high-pressure phase of cesium iodide. *Physical Review B*, 79(14), 144110.

Yoshihiro, T., Tsuneda, T., Yanagisawa, S., Yanai, T. & Hirao, K. (2004). A long-range-corrected time-dependent density functional theory. *The Journal of chemical physics*, 120(18), 8425-8433.

Yositaka, O. (1968). Energy bands in CsI. *Journal of the Physical Society of Japan*, 25(2), 469-480.

Young-Choon, P., Lim, I. & Yoon-Sup, L. (2012). Two-component spin-orbit effective core potential calculations with an all-electron relativistic program dirac. *Bulletin of the Korean Chemical Society*, 33(3), 803-808.

Yun-Ching, C., Wang, C., Yin, S., Hoffman, R. & Mott, A. (2013). Giant electro-optic effect in nanodisordered KTN crystals. *Optics letters*, 38(22), 4574-4577.

Zhibin, L., Johnson, R. & Zhigilei, L. (2008). Computational study of the generation of crystal defects in a bcc metal target irradiated by short laser pulses. *Physical Review B*, 77(21), 214108.

APPENDIX A

Workshops, Schools and Conferences and Publications.

A.1 Workshops

1. Khartoum Workshop on Advances in Materials Science (KWAMS13)- University of Khartoum, Sudan, $18^{th} Jan - 31^{st}$ Jan 2013.

2. Workshop on DFT and Quantum Chemistry - University of Eldoret, $6^{th} May - 11^{th}$ May 2013.

A.2 Schools and Conferences

1. University of Eldoret first interdisciplinary conference, 18^{th} - 19^{th} June 2015.

2. African School on Electronic Structure Methods and Applications - 2012- University of Eldoret, $28^{th} May - 8^{th}$ June 2012.

3. Quantum Monte Carlo Summer school - University of Eldoret, $9^{th} - 13^{th}$ March 2012.

A.3 Manuscript under preparation for submission to a journal.

Kirui, PC., Amolo, GO & Makau, NW. *Ab-Initio Study of intrinsic point defects in cesium iodide: A density functional theory.* To be submitted to a peer reviewed journal.

APPENDIX B

Optimization

B.1 Structural optimization

A mesh-pack of $6 \times 6 \times 6$ was appropriate.

B.1.1 K-Point optimization

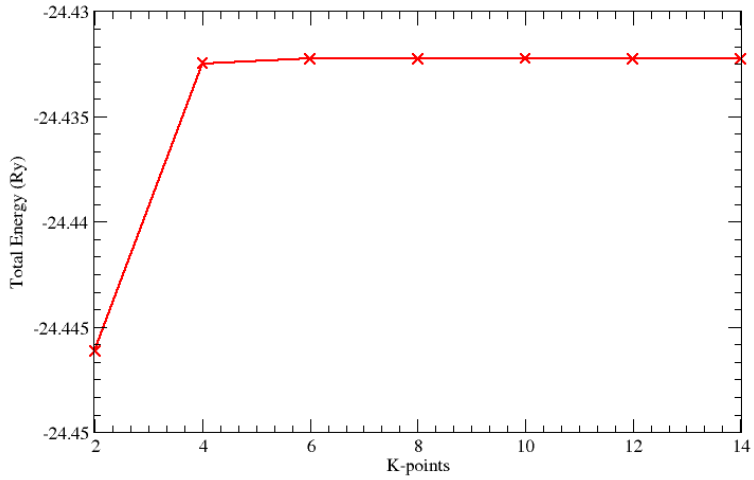

Figure B.1: A plot of total energy against k-points of cubic bulk CsI.

B.1.2 Lattice parameter optimization

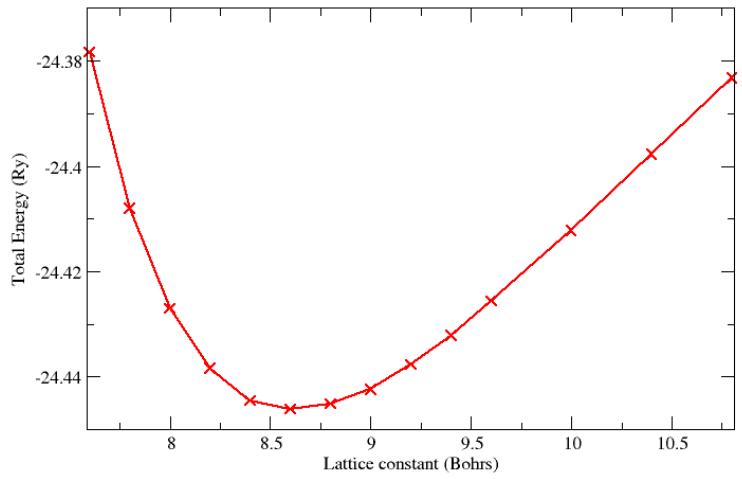

Figure B.2: A plot of total energy against lattice parameter of cubic bulk CsI

.

B.1.3 Plane wave energy cut-off

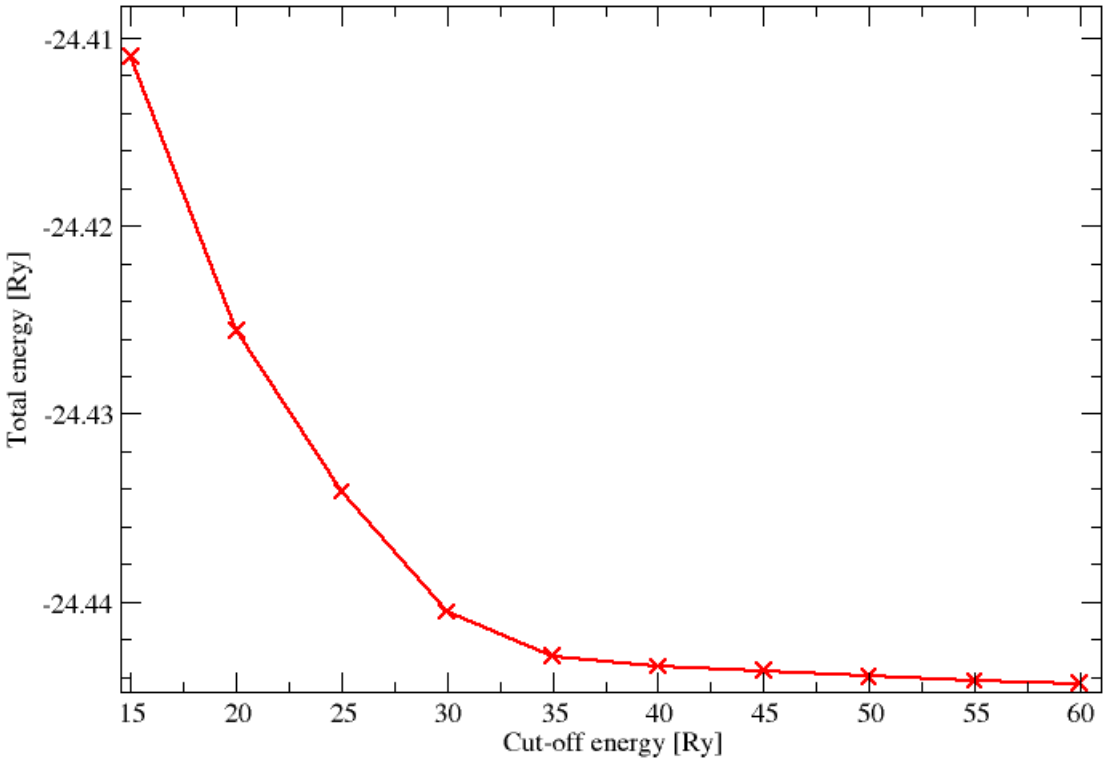

Figure B.3: A plot of total energy against cut-off energy of cubic bulk CsI.

APPENDIX C

Pseudopotentials

One of the ways of reducing computational cost and time is to use pseudopotentials without compromising the outcome of the calculations. This is because pseudopotentials consider the valence electrons only, excluding the inner core states and the strong potential that binds them to the nuclei (Milman, *et.al*., 2000). The core electrons in the core states have less influence on the properties of solids, but their proper inclusion into the pseudopotentials creates room for the sufficient use of plane wave basis sets in electronic structure calculations (Georg & Joubert, 1999). Among mostly used pseudopotentials are; norm-conserving, Ultra-soft and Projector augmented wave pseudopotentials. In this study,norm-conserving pseudopotentials whose charge contained inside the cut-off radius for the pseudo and all-electron wave functions is the same were preffered. These pseudopotentials were formulated by Vanderbilt and Bloch (David & King-Smith, 1998).

Table C.1: Pseudopotentials used

Atom	Pseudopotential
Cesium	Cs.Pbe−mt−bw.UPF
Iodine	I.Pbe−mt−bw.UPF

C.1 Cs.Pbe−mt−bw.UPF

These pseudopotentials for Cesium were generated using ld1 code by Brandon Wood (Materials Science, MIT). They were generation date in February 2002. The Pseudopotential was generated with a Scalar-Relativistic Calculation. (Peterson, 2003)

Table C.2: Cesium pseudopotential

nl	pn	l	occ	Rcut	Rcut US	E pseu
6S	0	0	0.50	0.0	0.0	0.0
6P	0	1	0.05	0.0	0.0	0.0
5D	0	2	0.05	0.0	0.0	0.0

Version Number	0
Element	Cs
Norm-Conserving pseudopotential	NC
Nonlinear Core Correction	T
PBE Exchange-Correlation functional	SLA, PW, PBE
Local Potential cutoff radius	0.0E+00
Z valence	1.0
Total energy	0.0
Number of points in mesh	537
Number of Wave functions	3
Number of Projectors	2
Maximum angular momentum component	2

C.2 I.Pbe−mt−bw.UPF

Generated using the fhi98pp code, written by Martin Fuchs. Generation date: 2006. The Pseudo was generated with a Full-Relativistic Calculation. (Sandro, *et.al.*, 2005)

Table C.3: Iodine pseudopotential

nl	pn	l	occ	Rcut	Rcut US	E pseu
5S	0	0	2	0.0	0.0	0.0
5P	0	1	5	0.0	0.0	0.0
5D	0	2	0	0.0	0.0	0.0
Version Number						0
Element						I
Norm - Conserving pseudopotential						NC
Nonlinear Core Correction						F
PBE Exchange-Correlation functional						SLA, PW, PBE
Z valence						7.0
Total energy						0.0
Max angular momentum component						2
Number of points in mesh						551
Number of Wave functions						3
Number of Projectors						2

APPENDIX D

Migration

D.1 Cesium migration energies

Table D.1: Cesium migration energies in three low index directions

Steps	Energy in directions (Ry)		
	$< 100 >$	$< 110 >$	$< 111 >$
0.10	-21252.96	-21252.98	-21251.97
0.15	-21252.95	-21252.97	-21252.98
0.20	-21251.77	-21251.31	-21251.15
0.25	-21252.93	-21251.33	-21251.14
0.30	-21252.96	-21251.32	-21251.16
0.35	-21252.97	-21252.98	-21252.98

D.2 Iodine migration energies

Table D.2: Iodine migration energies in three low index directions

Steps	Energy in directions (Ry)		
	$< 100 >$	$< 110 >$	$< 111 >$
0.42	-20968.2	-20967.9	-20967.5
0.48	-20967.0	-20966.2	-20968.5
0.50	-20967.7	-20965.9	-20967.7
0.53	-20967.9	-20966.2	-20966.4
0.58	-20968.3	-20967.9	-20967.5
0.60	-20968.4	-20968.2	-20968.2